ACCEPTED VERSION

Sylvan Elhay, Jochen Deuerlein, Olivier Piller and Angus R. Simpson
Graph partitioning in the analysis of pressure dependent water distribution systems

http://hdl.handle.net/2440/118080

Graph Partitioning in the Analysis of Pressure Dependent Water Distribution Systems

Sylvan Elhay[1]   Jochen Deuerlein[2]   Olivier Piller[3]   Angus R. Simpson[4]

June 6, 2017

Abstract

The forest core partitioning algorithm (FCPA) and the fast graph matrix partitioning algorithm (GMPA) have been used to improve efficiency in the determination of the steady-state heads and flows of water distribution systems which have large, complex network graphs. In this paper a single framework for the FCPA and the GMPA is used to extend their application from demand dependent models to pressure dependent models (PDMs). The PDM topological minor (TM) is characterized, important properties of its key matrices are identified and efficient evaluation schemes for the key matrices are presented. The TM captures the network's most important characteristics: it has exactly the same number of loops as the full network and the flows and heads of those elements not in the TM depend linearly on those of the TM. The inverse of the TM's Schur complement is shown to be the top, left block of the inverse of the full system Jacobian's Schur complement, thereby providing information about the system's essential behaviour more economically than is otherwise possible. The new results are applicable to other nonlinear network problems such as in gas, district heating and electrical distribution.

Keywords: graph partitioning, water distribution system, pressure dependent analysis, network security, water management, topological minor

INTRODUCTION

Water distribution system (WDS) analysis has, in the past, most often assumed demand dependent modeling (DDM) but the mathematically correct steady-state heads and flows solutions to some DDM problems are not physically realizable. This is because the model assumes that all the demands are fully delivered and sometimes the

---

[1]Visiting Research Fellow, School of Computer Science, University of Adelaide, South Australia, 5005, sylvan.elhay@adelaide.edu.au.
[2]Senior Researcher, 3S Consult GmbH, Karlsruhe, Germany & Adjunct Senior Lecturer, School of Civil, Environmental and Mining Engineering, University of Adelaide, South Australia, 5005.
[3]Senior Research Scientist, Irstea, Water Department, Bordeaux Regional Centre, Cestas F-33612, France.
[4]Professor, School of Civil, Environmental and Mining Engineering, University of Adelaide, South Australia, 5005.

mathematics requires that the associated pressures are negative. The steady-state pressures in a system give important information about spatial interconnections and the energy available in a system, so accurately modelled pressures are important to WDS designers. Pressure dependent modelling (PDM), in which the flow delivered at nodes is reduced below the desired demand if there is insufficient pressure, provides more realistic pressure calculations (and avoids physically unrealistic negative pressures at consumer demand nodes). Considerable effort has been devoted to issues in system resilience following natural disasters: damage assessment, system degradation or failure, network subgraph disconnection. The European ResiWater Project (ResiWater 2017) is an example of such research. Pressure dependent modelling plays an important role in addressing these problems. One point of focus in this paper is the extension of partition-based DDM problem solution improvements to PDM problems. Although the results are presented in the language of WDS analysis, they are equally applicable to nonlinear network problems such as arise in gas, district heating, mass-spring systems and electrical distribution (Dolan & Aldous 1993, Birkhoff 1963).

WDSs are often large and complex interconnected networks. When WDSs are optimised, for example in pipe sizing, operational control or when solving inverse problems such as calibration or state estimation, the computational cost of optimization can become a prohibitive, or at least a limiting, factor in the study. This has led to research into the partitioning of networks into smaller, manageable pieces. Early efforts concentrated on simplifying and decomposing the network graph and using meta-models (e.g. van Zyl et al. (2006)). In this approach, only main inlets (the water sources) and outlets (aggregated demands at town scale) were represented. When it is important to know the pressure levels in the network, partitioning methods were shown to be particularly useful for operational and reliability analyses (see Deuerlein (2008) and Simpson et al. (2014)). Within this approach, no skeletonization is made, but rather a domain decomposition is used to efficiently and exactly solve the nonlinear equations on smaller parts of the system while updating the full system's solutions with linear operations. The domain decomposition method by Giustolisi & Laucelli (2011) lumps all the interior nodes to the two end nodes (for each link) and arrives at an approximate solution that is decoupled from interior nodes. They solve the nonlinear hydraulic equations on the simplified network. Unlike the Deuerlein et al. (2016) solution, their method suffers from some level of approximation in the PDM case where, as will be explained in this paper, it is impossible to decouple solving for the interior forest nodes from the rest of the solution process without making some approximations. Giustolisi & Laucelli (2011), however, did not propose disaggregation. In a separate development, the Reformulated Cotree Flows Method (RCTM) of Elhay et al. (2014) partitions the network's arc-node incidence matrix (ANIM: the terms 'arc' and 'link' are used interchangeably in this paper) into trapezoidal form and uses that form in the design of an efficient null-space method.

Elsewhere the effort has focused on network partitioning to address problems such as failure, security and reliability, detection of sources of contamination intrusions and sensor placement. In some cases partitioning is used for sectorization, a technique that can assist in network management, limit water age and that can improve the effectiveness of measurement in leak detection. For example, Estrada (2006) investigated network vulnerability by considering

"good expansion" and "degree distribution" properties of networks. Tzatchkov et al. (2006) describe a sectorization technique which divides large, highly interconnected city distribution networks into smaller networks, each with one or at most two supply points, thereby localizing any disruptions to supply. Similarly, Perelman et al. (2015) investigated three different schemes for partitioning a WDS into smaller, almost independent subzones with approximately balanced loads and minimal interconnections while Perelman & Ostfeld (2011) investigated node clustering through connectivity analysis. Di Nardo et al. (2016) considered network partitioning through weighted spectral clustering and Herrera et al. (2010) proposed semi-supervised learning strategies in the application of spectral clustering. In a recent interesting paper, Yazdani et al. (2011) "employ the link-node representation of water infrastructures and exploit a wide range of advanced and emerging network theory metrics and measurements to study the building blocks of the systems and quantify properties such as redundancy and fault tolerance". Laucelli et al. (2012) used a stochastic variation of nodal demands, background leakages, pipe resistances, etc. in an attempt to identify those nodes which are least capable of delivering the required capacity. They conclude that the DDM approach is inferior to the PDM approach for this purpose. Lan et al. (2015) propose an optimization scheme which anticipates a restricted set failures and builds into the optimized network design the capacity to handle those particular failures. For a comprehensive review the major concepts and results recently achieved in the study of the structure and dynamics of complex networks see Boccaletti et al. (2006).

In contrast with the methods described above, partitioning is used in this paper (i) to improve solution methods without using approximations such as skeletonization or clustering and (ii) to provide analysis data which is exactly what one would get by solving the full network system but which is found much more economically by examining what could be considered the kernel of the system (once again without approximation).

Various authors have investigated ways to accelerate the hydraulic solution algorithms by improving the efficiency of the solution methods for the linear systems involved in the Global Gradient Algorithm (GGA) of Todini & Pilati (1988). It has become commonly accepted that the (direct) sparse Cholesky (SC) method with node reordering (NR) is superior to other classical direct and indirect methods for solving these linear systems. Recently, it was shown that Algebraic Multigrid Methods can be applied to these problems (Zecchin et al. 2012) and they were shown to outperform the SC+NR method for large networks. On the other hand, other results show that the SC+NR method may be significantly improved for large systems by using a nested dissection, node reordering method (Giustolisi et al. 2011).

In other developments, Diao et al. (2014) consider the partitioning of the ANIM into the shape of a block arrow matrix, sometimes called a block bordered matrix, in order to speed up the analysis and Chiplunkar et al. (1990) used an approach reminiscent of the null space method but with damping applied to the Newton method. Their partitioning into a spanning tree and cotree is similar to that of the RCTM.

More recently, efforts by Puust et al. (2011) and Crous et al. (2012) to speed up hydraulic modelling have considered

solving the system hydraulics on parallel architectures and using graphical processing units, both of which are now commonly found in personal computers. Not surprisingly, parallelisation based on the GGA has been shown to speed up simulations for large networks (see e.g. Guidolin et al. (2011) and Wu & Lee (2011)). Preliminary results based on models of real networks show than the sparse Cholesky method is superior to the conjugate gradient method, and that the parallelized code is faster than the serial code for networks with more than 4,000 nodes. For small and medium size networks there is no gain in computation time because of the cost of inter-processor communication. However, for networks of more than 4,000 nodes, there is a slight reduction in computation time (Piller et al. 2012).

The first partition-based acceleration strategy of present interest for DDM problems is the work of Simpson et al. (2014) which introduced the Forest Core Partitioning Algorithm (FCPA) that separates the linear forest heads and flows calculations from the nonlinear core heads and flows calculations. This speeds up the solution process for DDM networks which have a significant forest subgraph element. Later, in Deuerlein et al. (2016), a fast Graph Matrix Partitioning Algorithm (GMPA) for solving the DDM water distribution system equations was proposed. This development also essentially identifies the linear part of the network core and treats it with linear processes rather than the more time-consuming nonlinear solvers. The truly nonlinear part of the network core, the *topological minor* identified in Deuerlein et al. (2016) and sometimes called the supergraph, can be thought of as giving a condensed view of the network's main elements.

The flows in a DDM network's external forest satisfy a linear system and can be determined a priori. The heads of the DDM network's external forest can be found a posteriori. Although the heads and flows of a PDM network's external and internal forests cannot be determined a priori, they follow from the heads and flows of the topological minor (which are modelled by a nonlinear system) by a linear process. The facts that (i) the pipes and nodes in the internal and external forests exhibit behaviour that depends linearly on the behaviour of the pipes and nodes in the topological minor and (ii) the topological minor has precisely the same number of loops as the full network (and it is the loops which introduce the nonlinearity into the problem) means that, in some sense, the topological minor of a network drives the key behavioural characteristics of the whole network (Deuerlein et al. 2016). Thus, in many instances the topological minor encapsulates the most important behavioural elements that interest the network engineer. The matrices in the topological minor are frequently very much smaller that the corresponding matrices in the full system. They can therefore offer much more manageable analysis elements when dealing with networks which have very large complex graphs.

The French-German collaborative research project SMaRT-Online^{WDN}, jointly funded by the French National Research Agency and the German Federal Ministry of Education and Research, has investigated the importance of the topological minor in real-time monitoring, water security and contamination response. In one of that project's papers, Deuerlein et al. (2014) propose graph decomposition as a basis for the simplification and enhancement of solution algorithms for problems related to the management of water supply security. That approach allows streamlined views

of the network and fast identification of affected areas. The technique has application in areas which include sensor placement, source identification and decision support for response actions.

One objective of the present paper is to provide a single framework for both the FCPA and GMPA and to extend their applicability to PDM problems. The single framework developed in this paper is applicable to both DDM and PDM problems. Importantly, the methods presented make no approximations to the topology of the network: there is no skeletonization or lumping and the heads and flows results, which are produced, are precisely those obtained by solving for the whole network. The partitioning framework presented in this paper for PDM problems separates the linear and nonlinear parts of the problem into a global part (the topological minor) and a local part (the internal and external forests) just as it does for DDM problems. However, the coupling that exists between the delivered flows and the pressures in PDM problems updates both these quantities at each iteration in the solution process.

Another objective in this paper is the characterization and fundamental properties of the matrices in the topological minor for the PDM case. It is seen that knowledge of these properties leads to significant computational savings when dealing with the topological minors. It is shown that one of the matrices central to operating with the topological minor system has a block diagonal structure. This decoupling means that computation with this matrix, and therefore much of the analysis, is well-suited to parallel and distributed computing. From the point of view of serial computing, this property means that larger network problems can be analysed on a computing platform with given memory capacity.

The rest of this paper is organized as follows: the next section deals a brief review of the partitioning schemes which are brought together in this study and outlines the main contributions of the paper. The section following sets out some definitions and notation and the section following that describes the unifying framework that brings together the partitioning techniques published previously by the authors. The unifying framework is then applied to PDM problems and an example network provided to illustrate the technique. Some applications are briefly outlined and then some conclusions are drawn. The last part of the paper is made up of appendices which have various proofs, briefly discuss numerical considerations and software and indicate the availability of the data on which the examples in the paper rely.

NETWORK PARTITIONING

Much of the research effort for methods which determine the steady-state heads and flows of WDSs has focused on exploiting the very structured nature of the nonlinear equations which model the system. The diagonality of the head loss submatrix and the sparseness of the ANIM, which are the main components of the DDM, have been at the heart of new approaches that deliver the solutions to the systems much more quickly than would be otherwise possible.

For many real networks, what appears at first sight to be a fully nonlinear problem turns out, on closer inspection, to be partly nonlinear and partly linear. Partitioning the network's ANIM can lead to savings in computation time

that are significant where much of the network problem is linear such as, for example, in all-pipes models which include house connection pipes. The more time-consuming nonlinear solvers have to deal only with that part of the network which is truly nonlinear.

Partitioning schemes have also been used to solve the system equations as a null space problem (see e.g. (Elhay et al. 2014)) rather than as the more often preferred range space approach of the GGA. The null space approach can deliver significant benefits in networks with fewer loops. The development of the partitioning schemes discussed in this paper began with Deuerlein (2006) showing that, for DDM problems, the hydraulic steady-state equations of the forest can be solved independently from the core. Then the idea of separating the linear and nonlinear parts of the DDM problem so that the nonlinear solver need only be applied to the smaller nonlinear part while the linear part was solved with linear techniques was extended by the FCPA. The FCPA partitions the graph of the network into an external forest and a core. The forest, in this context, is the union of all the trees that connect to nodes in the core and the core is the part of the graph which is composed of one or more loop blocks possibly connected by bridge components. That work was further extended with the development of the GMPA by Deuerlein et al. (2016) who showed that the core of the FCPA can be further subdivided into bridge components and looped blocks. Many looped cores have nodes in series: nodes which are part of a loop but which have index two. Following the nomenclature introduced in Deuerlein et al. (2016), a set of such nodes in series, each together with one pipe to which it is connected, is called an *internal tree* and the union of all such trees in a graph is called the graph's *internal forest*. The GMPA partitions the nodes of the blocks into supernodes (degree > 2) and internal tree nodes (degree $= 2$), i.e. into two parts: (i) a core (which is often small), called the topological minor, and (ii) the internal forest. An internal tree running between nodes A and B is considered to have a pseudo-link, called a superlink, connecting A and B. The superlink, the *internal tree branches* and one arbitrarily chosen *internal cotree link*, together form a pseudo-loop. The supernodes, the tree's end nodes A and B, form part of the topological minor. The nonlinear solver is required only for the blocks in such a system and this often results in a nonlinear part of the DDM problem with significantly smaller dimension.

The main results in this paper concern

(a) the development of a unified framework for three permutation schemes: FCPA, GMPA and the Schilders factorization

(b) the extension of the FCPA and GMPA schemes for DDM problems to the case of PDM problems

(c) the presentation of a network's topological minor system in a unified setting that includes both the FCPA and the GMPA

(d) the properties of the topological minor system and the matrices which define it

(e) the algorithmic exploitation of a network graph's topological minor and it's ANIMs, and

187 (f) the proof that the inverse of the topological minor's Schur complement is precisely the $(1,1)$ block of the inverse

188 of the full Jacobian's Schur complement. Point (e) bears on the sensitivity analysis of large networks by using

189 the sensitivity matrices for the much smaller topological minor. It also has application to the problems of sensor

190 placement and calibration.

191 Although the term 'links' in this paper applies to pipes, all the results, with slight generalization, apply if the

192 links include pumps, valves and control devices. Details of numerical considerations and the data for the networks

193 considered in this paper can be found below in the section entitled "Numerical considerations and software".

194

195 **DEFINITIONS AND NOTATION**

196 Consider a DDM or PDM WDS that has n_p links, sometimes referred to as arcs, and n_j nodes, sometimes referred

197 to as vertices, at which the heads are unknown. Denote by $\boldsymbol{q} = (q_1, q_2, \ldots, q_{n_p})^T \in \mathbb{R}^{n_p}$ the vector of unknown flows in

198 the system, $\boldsymbol{h} = (h_1, h_2, \ldots, h_{n_j})^T \in \mathbb{R}^{n_j}$ the unknown heads at the nodes in the system and $\boldsymbol{r}(\boldsymbol{q}) = (r_1, r_2, \ldots, r_{n_p})^T$

199 the vector of pipe resistance factors. Let $n_f \geq 1$ denote the number of reservoirs or fixed-head nodes in the system,

200 let $\boldsymbol{A}$ denote the $n_p \times n_j$, full rank, unknown-head ANIM, let $\boldsymbol{A}_f$ denote the ANIM for the fixed-head nodes and let

201 $\boldsymbol{e}_\ell$ denote the elevations of the fixed-head nodes. Denote by n the exponent used in the head loss formula: $n = 2$ for

202 the Darcy-Weisbach model and $n = 1.852$ for the Hazen-Williams model. Furthermore, denote by $\boldsymbol{G} \in \mathbb{R}^{n_p \times n_p}$ the

203 diagonal matrix whose diagonal elements are defined as $[\boldsymbol{G}]_{jj} = r_j|q_j|^{n-1}$. Then, $\boldsymbol{Gq}$ is the vector whose elements

204 model the head losses of the pipes in the system. In general, (e.g. for the Darcy-Weisbach formulae) $\boldsymbol{r} = \boldsymbol{r}(\boldsymbol{q})$

205 but for the Hazen-Williams formula $\boldsymbol{r}$ is independent of $\boldsymbol{q}$. Denote the vector of the fixed demands at the nodes

206 with unknown-head by $\boldsymbol{d} = (d_1, d_2, \ldots, d_{n_j})^T \in \mathbb{R}^{n_j}$. Denote by $\boldsymbol{\omega}(\boldsymbol{h}, \boldsymbol{d}) \in \mathbb{R}^{n_j}$ the vector whose elements are the

207 consumption function values at the n_j nodes of the system. Denote $\boldsymbol{\theta} = (D_1, D_2, \ldots, D_{n_p})^T \in \mathbb{R}^{n_j}$ the vector of pipe

208 diameters. Throughout what follows, the symbol $\boldsymbol{O}$ denotes a zero matrix and $\boldsymbol{o}$ denotes a zero column vector of

209 appropriate dimension for the particular case. Furthermore, it will be assumed that any matrix inverses which are

210 shown do exist.

211 Turning now to PDM problems in particular, let h denote the head at a node, h_m denote that node's minimum

212 pressure head, h_s denote its service pressure head and d denote its demand. Denote also $z(h) = (h - h_m)/(h_s - h_m)$.

213 Suppose that $\gamma(t)$ is a bounded, smooth, monotonically increasing function which maps the interval $[h_m, h_s] \to [0, 1]$.

214 The consumption, or demand, function at a node is defined by

215
$$
\boldsymbol{\omega}(h, d) = \begin{cases} 0 & \text{if } z(h) \leq 0 \\ d\gamma(z(h)) & \text{if } 0 < z(h) < 1 \\ d & \text{if } z(h) \geq 1 \end{cases}.
\tag{1}
$$

216 The steady-state flows and heads in a WDS with PDM are usually found as the zeros of the nonlinear system of the

$n_p + n_j$ equations

$$\boldsymbol{f}(\boldsymbol{q}, \boldsymbol{h}) = \begin{pmatrix} \boldsymbol{G}(\boldsymbol{q})\boldsymbol{q} - \boldsymbol{A}\boldsymbol{h} - \boldsymbol{a} \\ -\boldsymbol{A}^T\boldsymbol{q} - \boldsymbol{\omega}(\boldsymbol{h}, \boldsymbol{d}) \end{pmatrix} \overset{\text{def}}{=} \begin{pmatrix} \boldsymbol{\rho}_e \\ \boldsymbol{\rho}_c \end{pmatrix} = \boldsymbol{o}, \tag{2}$$

where $\boldsymbol{a} = \boldsymbol{A}_2 \boldsymbol{e}_\ell$, $\boldsymbol{\rho}_e$ is called the energy residual and $\boldsymbol{\rho}_c$ is called the continuity residual. A natural way to approach the solution of (2) is to use a Newton iteration based on the Jacobian of $\boldsymbol{f}$,

$$\boldsymbol{J}(\boldsymbol{q}, \boldsymbol{h}) = \begin{pmatrix} \boldsymbol{F}(\boldsymbol{q}) & -\boldsymbol{A} \\ -\boldsymbol{A}^T & -\boldsymbol{E}(\boldsymbol{h}) \end{pmatrix}, \tag{3}$$

where $\boldsymbol{F}(\boldsymbol{q})$ and $\boldsymbol{E}(\boldsymbol{h})$ are diagonal matrices which are such that (i) the terms on the diagonal of $\boldsymbol{F}(\boldsymbol{q})$ are the q-derivatives of the corresponding terms in $\boldsymbol{G}(\boldsymbol{q})\boldsymbol{q}$ and (ii) the terms on the diagonal of $\boldsymbol{E}$ are the h-derivatives of the corresponding terms in $\boldsymbol{\omega}(\boldsymbol{h}, \boldsymbol{d})$. It is assumed in what follows that the diagonal terms of $\boldsymbol{F}$ and $\boldsymbol{E}$ are non-negative. The Newton iteration for (2) proceeds by taking given starting values $\boldsymbol{q}^{(0)}$, $\boldsymbol{h}^{(0)}$ and repeatedly computing, for $m = 0, 1, 2, \ldots$, the iterates $\boldsymbol{q}^{(m+1)}$ and $\boldsymbol{h}^{(m+1)}$ from

$$\begin{pmatrix} \boldsymbol{F}(\boldsymbol{q}^{(m)}) & -\boldsymbol{A} \\ -\boldsymbol{A}^T & -\boldsymbol{E}(\boldsymbol{h}^{(m)}) \end{pmatrix} \begin{pmatrix} \boldsymbol{q}^{(m+1)} - \boldsymbol{q}^{(m)} \\ \boldsymbol{h}^{(m+1)} - \boldsymbol{h}^{(m)} \end{pmatrix} = - \begin{pmatrix} \boldsymbol{\rho}_e^{(m)} \\ \boldsymbol{\rho}_c^{(m)} \end{pmatrix}$$

until, if the iteration converges, the relative difference between successive iterates is sufficiently small. For many engineering settings a heads tolerance of 1 mm and a flows tolerance of 10^{-3} L/s is usually sufficient. In this research setting the authors have used relative stopping tolerances of 10^{-10} to ensure that the numerical behaviour of the methods is clearly exposed. In what follows the Jacobian $\boldsymbol{J}^{(m)}$ will be denoted simply by $\boldsymbol{J}$ where there is no ambiguity. In the *damped* Newton method the iterative scheme is then formally, provided that $\boldsymbol{J}$ is invertible,

$$\begin{pmatrix} \boldsymbol{q}^{(m+1)} \\ \boldsymbol{h}^{(m+1)} \end{pmatrix} = \begin{pmatrix} \boldsymbol{q}^{(m)} \\ \boldsymbol{h}^{(m)} \end{pmatrix} - \sigma^{(m+1)} \boldsymbol{J}^{-1} \begin{pmatrix} \boldsymbol{\rho}_e^{(m)} \\ \boldsymbol{\rho}_c^{(m)} \end{pmatrix} \tag{4}$$

where $\sigma^{(m+1)}$ is a step-length variable used to assist convergence. Denote

$$\begin{pmatrix} \boldsymbol{c}_q^{(m+1)} \\ \boldsymbol{c}_h^{(m+1)} \end{pmatrix} = \boldsymbol{J}^{-1} \begin{pmatrix} \boldsymbol{\rho}_e^{(m)} \\ \boldsymbol{\rho}_c^{(m)} \end{pmatrix}.$$

Once the vector $\begin{pmatrix} \boldsymbol{c}_q^T & \boldsymbol{c}_h^T \end{pmatrix}^T$ is found as the solution of

$$\boldsymbol{J} \begin{pmatrix} \boldsymbol{c}_q^{(m+1)} \\ \boldsymbol{c}_h^{(m+1)} \end{pmatrix} = \begin{pmatrix} \boldsymbol{\rho}_e^{(m)} \\ \boldsymbol{\rho}_c^{(m)} \end{pmatrix}, \tag{5}$$

the new iterates can be computed using (4). The block equations for (5) are, simplifying the notation again,

$$\boldsymbol{F}\boldsymbol{c}_q - \boldsymbol{A}\boldsymbol{c}_h = \boldsymbol{\rho}_e \quad \text{and} \quad -\boldsymbol{A}^T\boldsymbol{c}_q - \boldsymbol{E}\boldsymbol{c}_h = \boldsymbol{\rho}_c. \tag{6}$$

Multiplying the first equation in (6) on the left by $\boldsymbol{A}^T \boldsymbol{F}^{-1}$ and adding the result to the second equation gives

$\boldsymbol{c}_h^{(m+1)} = -\left(\boldsymbol{E} + \boldsymbol{A}^T \boldsymbol{F}^{-1} \boldsymbol{A}\right)^{-1}\left(\boldsymbol{A}^T \boldsymbol{F}^{-1} \boldsymbol{\rho}_e + \boldsymbol{\rho}_c\right)$ and $\boldsymbol{c}_q^{(m+1)} = \boldsymbol{F}^{-1}(\boldsymbol{A}\boldsymbol{c}_h + \boldsymbol{\rho}_e)$.

Thus, when the terms, $\boldsymbol{c}_q^{(m+1)}$, and $\boldsymbol{c}_h^{(m+1)}$, have been found, the new iterate can be computed as

$$\begin{pmatrix} \boldsymbol{q}^{(m+1)} \\ \boldsymbol{h}^{(m+1)} \end{pmatrix} = \begin{pmatrix} \boldsymbol{q}^{(m)} \\ \boldsymbol{h}^{(m)} \end{pmatrix} - \sigma^{(m+1)} \begin{pmatrix} \boldsymbol{c}_q^{(m+1)} \\ \boldsymbol{c}_h^{(m+1)} \end{pmatrix}. \tag{7}$$

The system (7) is the PDM counterpart of the GGA method for the DDM problem. The method is reliable and robust, provided a suitable line search algorithm such as that proposed by Goldstein is used to choose $\sigma^{(m+1)}$ (see Elhay et al. (2016) for details).

The results presented throughout this paper are applicable to demand driven model (DDM) problems by replacing the consumption function $\boldsymbol{\omega}(\boldsymbol{h}, \boldsymbol{d})$ by the fixed demands $\boldsymbol{d}$ throughout. This has the consequence of making $\boldsymbol{E} = \boldsymbol{O}$ and redefining $\boldsymbol{\rho}_c$ in (2) as $\boldsymbol{\rho}_c = -\boldsymbol{A}^T \boldsymbol{q} - \boldsymbol{d}$. DDM problems seldom need line search methods and so the step length variable would take the value $\sigma = 1$ in (4), further simplifying the system.

Note that the Schur complement inverse $-\boldsymbol{S}_F^{-1}$ of $\boldsymbol{J}$, where $\boldsymbol{S}_F$ is defined by $\boldsymbol{S}_F = \boldsymbol{E} + \boldsymbol{A}^T \boldsymbol{F}^{-1} \boldsymbol{A} \in \mathbb{R}^{n_j \times n_j}$ is central to the theory of PDM head and flow first-order sensitivities to changes in network parameters (Piller et al. 2016). Thus, the matrix $-\boldsymbol{S}_F^{-1}$ can be seen in Piller et al. (2016) to be the main component of the matrices of first-order sensitivities of the PDM heads and flows in the network to changes in demands, relative roughnesses, resistance factors and diameters.

In what follows, for simplicity and where there is no ambiguity, a matrix will be referred to as a Schur complement even though, strictly speaking, its negative is the Schur complement.

A UNIFIED FRAMEWORK FOR THE FCPA AND GMPA PARTITIONINGS

The following terminology will be used in this paper. A tree is a connected graph that has no loops. A tree with at least one leaf node that is connected to a node in the core, called its root node, is called an external tree. Note that the root node of a tree is not a part of the tree incidence matrix and that the ANIM of a tree is always square and invertible (Diestel 2010). A tree that is part of a looped network (i.e. a set of nodes in series together with one pipe for each) will be called an internal tree. Furthermore, the ANIM of a tree can always have its rows and columns permuted to lower triangular form. It will be assumed in what follows that the matrix $\boldsymbol{L}$ of (8) is the ANIM for a tree or a union of trees (either external, internal or both) and that it has been permuted to lower triangular form.

Three different permutation schemes

The permutation schemes used in the FCPA, GMPA and the RCTM, from which the main results of the paper follow, can be put into a common framework. To do this, the rows and columns of a ANIM, $\boldsymbol{A}$, are permuted by

²⁷¹ (orthogonal) permutation matrices, $\boldsymbol{P}$ and $\boldsymbol{R}$, to give the block structure

$$
\boldsymbol{PAR} = \begin{array}{c} \\ n_1 \\ n_2 \end{array} \overset{\begin{array}{cc} n_3 & n_1 \end{array}}{\begin{pmatrix} \boldsymbol{A}_{11} & \boldsymbol{L} \\ \boldsymbol{A}_{21} & \boldsymbol{A}_{22} \end{pmatrix}} \tag{8}
$$

²⁷³ where (i) $\boldsymbol{A}_{11} \in \mathbb{R}^{n_1 \times n_3}$, (ii) $\boldsymbol{A}_{22} \in \mathbb{R}^{n_2 \times n_1}$, (iii) $\boldsymbol{A}_{21} \in \mathbb{R}^{n_2 \times n_3}$ and (iv) $\boldsymbol{L} \in \mathbb{R}^{n_1 \times n_1}$ is invertible. There always exists
²⁷⁴ such a set of permutations if $\boldsymbol{A}$ has full rank, a natural requirement for the WDSs under consideration. There are
²⁷⁵ many permutations of the form (8) three of which will be now be discussed in more detail.

²⁷⁶ **The FCPA permutations:** The FCPA, produces a partitioning of the form of (8) in which (i) $\boldsymbol{L}$, is a lower
²⁷⁷ triangular ANIM which represents the external forest, (ii) $\boldsymbol{A}_{11}$ is the ANIM which holds the pipes of the external
²⁷⁸ forest which connect to the nodes of the core, (iii) $\boldsymbol{A}_{21}$ is the ANIM of the core and (iv) $\boldsymbol{A}_{22} = \boldsymbol{O}$, since no pipes in
²⁷⁹ the core connect to nodes of the external forest. Note that the node in the core to which a tree attaches, referred to
²⁸⁰ as the 'root node of the tree', is actually part of the core but not the forest.

²⁸¹ **The GMPA permutations:** By contrast with the FCPA, the GMPA which is applied after the FCPA has
²⁸² partitioned the external forest of the graph from its core, produces a partitioning of the form of (8) in which (i) $\boldsymbol{L}$
²⁸³ can be chosen to be, in addition to lower triangular, also bidiagonal, (ii) $\boldsymbol{A}_{11}$ represents the links in the internal
²⁸⁴ forest which connect to supernodes in the core, (iii) $\boldsymbol{A}_{21}$ represents the links which are internal cotree chords and the
²⁸⁵ supernodes (iv) $\boldsymbol{A}_{22}$ represents the nodes in the trees to which the internal tree chords connect. Property (i) follows
²⁸⁶ from the fact that all the nodes in the internal forest have index two since they represent nodes in series. Deuerlein
²⁸⁷ et al. (2016), in order to simplify the exposition, did not consider the external forest. They assumed that the external
²⁸⁸ forest had already been separated from the network by the FCPA.

²⁸⁹ **The Schilders permutations:** The Schilders permutations used in the RCTM to generate a matrix $\boldsymbol{L}$, which is
²⁹⁰ the lower triangular spanning tree for the network graph, and $\boldsymbol{A}_{22}$ which is the network graph's co-tree. Matrices $\boldsymbol{A}_{11}$
²⁹¹ and $\boldsymbol{A}_{21}$ are null in this case.

²⁹³ **The unified framework**

²⁹⁴ The properties of the submatrices of the permuted ANIM, $\boldsymbol{A}$, are of considerable interest in this context and are
²⁹⁵ discussed in more detail in what follows. In order to generalize the FCPA and GMPA results to PDM problems
²⁹⁶ it is necessary to explicitly include the permutations which involve both the external and internal forests in the
²⁹⁷ partitioning. One of the contributions of this paper is to present a method for achieving this in a new unified setting.
²⁹⁸ The permutations required for this can be found in three steps as follows.

The FCPA step

301 The ANIM, $\boldsymbol{A}$, is first partitioned using the FCPA into the form

$$\widetilde{\boldsymbol{P}}\boldsymbol{A}\widetilde{\boldsymbol{R}} = \begin{array}{c} \\ \widetilde{\boldsymbol{n}}_1 \\ \widetilde{\boldsymbol{n}}_2 \end{array} \begin{array}{c} \widetilde{\boldsymbol{n}}_3 \quad\; \widetilde{\boldsymbol{n}}_1 \\ \left(\begin{array}{cc} \widetilde{\boldsymbol{A}}_{11} & \widetilde{\boldsymbol{L}} \\ \widetilde{\boldsymbol{A}}_{21} & \boldsymbol{O} \end{array} \right) \end{array}. \tag{9}$$

303 Here, $\widetilde{\boldsymbol{n}}_1$ is the number of pipes (and nodes) in the external forest, $\widetilde{\boldsymbol{n}}_2$ is the number of pipes in the core and $\widetilde{\boldsymbol{n}}_3$ is

304 the number of nodes in the core. The matrix in (9) is shown schematically in the major blocking of Fig. 3.

305 The network shown in Fig. 1 was derived from a network used in Deuerlein et al. (2016) to illustrate the GMPA

306 by adding an external forest comprising pipes 11, 12 and 13 and nodes 9, 10 and 11. All the pipes in the network

307 have diameters 300 mm, lengths 1000 m, roughnesses 0.25 mm, and the nodes have demands of 50 L/s and zero

308 elevation. The source head is 100 m. All the nodes have the (same) consumption function given by Eq. (1) with

309 $\gamma(t) = t^2(3 - 2t)$. The service pressure head is set at $h_s = 20$ m and the minimum pressure head is set at $h_m = 0$

310 m. Solved as a PDM problem the steady-state solution delivers 43% of the required demand. The steady-state flows,

311 heads, nodal deliveries, demands and deliveries as percentages of demands are shown in Table 6. This network is used

312 in what follows to illustrate, among other things, the stages in the partitioning schemes. Its ANIM is given in Table

313 1.

314 The right-hand matrix in (9) (i.e. after the FCPA has been applied) for the network in Fig. 1 is shown in Table 2.

315

316 **The combined FCPA and GMPA steps**

317 Then, the FCPA core ANIM, $\widetilde{\boldsymbol{A}}_{21}$, is further partitioned by the GMPA into the form

$$\widehat{\boldsymbol{P}}\widetilde{\boldsymbol{A}}_{21}\widehat{\boldsymbol{R}} = \begin{array}{c} \\ \widehat{n}_1 \\ \widehat{n}_2 \end{array} \begin{array}{c} \widehat{n}_3 \quad\;\; \widehat{n}_1 \\ \left(\begin{array}{cc} \widehat{\boldsymbol{A}}_{11} & \widehat{\boldsymbol{L}} \\ \widehat{\boldsymbol{A}}_{21} & \widehat{\boldsymbol{A}}_{22} \end{array} \right) \end{array}. \tag{10}$$

319 where the nodes of index two (the nodes of the internal forest) are represented in $\widehat{\boldsymbol{L}}$ and $\widehat{\boldsymbol{A}}_{22}$. The matrix in (10) is

320 shown schematically in the $(2,1)$ major block of Fig. 3. Here, $\widehat{n}_1$ is the number of pipes (and nodes) in the internal

321 forest, $\widehat{n}_2$ is the number of pipes in the topological minor and $\widehat{n}_3$ is the number of supernodes. The matrix after both

322 sets of permutations is shown in Fig. 3: the FCPA permutations are shown as π_s, π_p for the pipes and π_v and π_t for

323 the nodes and the $\widetilde{\boldsymbol{A}}_{11}$ block is partitioned into two column blocks as shown in Fig. 3 and the permuted matrix $\widetilde{\boldsymbol{A}}_{21}$

324 of (10) for Fig. 1 is shown in Table 3.

The Schilders permutations

Next, the Schilders (2009) factoring which was used in the RCTM is applied to permute the rows and columns of the submatrix made of the blocks shown on the left in (11) to get

$$\overline{P}\begin{pmatrix} \widetilde{A}_{11\_b} & \widetilde{L} \\ \widehat{L} & \\ \widehat{A}_{22} & O \end{pmatrix}\overline{R} = \begin{pmatrix} L \\ A_{22} \end{pmatrix} \tag{11}$$

which are the right-hand blocks of the final form (8), also shown in Fig. 4. The dimensions of the blocks in (11) can be seen in Fig. 3. The Schilders factoring merges the spanning trees of the internal and external forests into a single invertible lower triangular matrix L. Furthermore, A_{22} is the matrix with the co-trees of the forest but, since L represents the nodes in the external *and* internal forests, it is not necessarily bidiagonal. In fact, L is block diagonal with lower triangular blocks. Now, the columns of L and A_{22} represent the nodes in the internal and external forests, the rows of A_{11} and L represent the links in the internal and external forests, the columns of A_{11} and A_{21} represent the supernodes of the core and the rows of A_{21} and A_{22} represent the cotree chords of the core. The submatrix shown on the left of (11) for the network in Fig. 1, before the permutations $\overline{P}$ and $\overline{R}$ are applied to it, is shown in Table 4.

The final permuted ANIM matrix for the network shown in Fig. 1 is displayed in Table 5.

In summary, the three steps of the unified approach are: (i) apply the FCPA to the ANIM A, (ii) apply the GMPA to the (FCPA) core and (iii) apply the Schilders factoring to get a single lower triangular matrix which is the spanning tree for the external and internal forests.

Why the FCPA should come first

Applying the GMPA before the FCPA or applying only either the FCPA or the GMPA can produce a larger than necessary topological minor and is therefore not recommended. Furthermore, applying only the GMPA to a network which has an external forest loses the FCPA advantage of being able to determine the external forest flows (linearly) at the outset in DDM problems.

APPLYING THE UNIFIED FRAMEWORK TO PDM PROBLEMS

The partitioning of the graph's ANIM suggests a conformal partitioning of the system's full Jacobian which allows the generalization to PDM problems and which is the basis for all the results that follow in this paper. Let P be the row permutation matrix and R be the column permutation matrix which together incorporate both the forest-core and graph matrix partitionings for the matrix A and which lead to the form shown in (8). Then, partitioning F and

$_{354}$ **E** conformally with (8) allows the following partitioning of **J**

$$
\begin{pmatrix} \boldsymbol{P} & \\ & \boldsymbol{R}^T \end{pmatrix} \begin{pmatrix} \boldsymbol{F} & -\boldsymbol{A} \\ -\boldsymbol{A}^T & -\boldsymbol{E} \end{pmatrix} \begin{pmatrix} \boldsymbol{P}^T & \\ & \boldsymbol{R} \end{pmatrix}
$$

$$
= \begin{pmatrix} \boldsymbol{PFP}^T & -\boldsymbol{PAR} \\ -\boldsymbol{R}^T\boldsymbol{A}^T\boldsymbol{P}^T & -\boldsymbol{R}^T\boldsymbol{ER} \end{pmatrix}
$$

$$
= \begin{array}{c} \\ n_1 \\ n_2 \\ n_3 \\ n_1 \end{array}
\begin{array}{cccc} n_1 & n_2 & n_3 & n_1 \\
\begin{pmatrix} \boldsymbol{F}_1 & \boldsymbol{O} & -\boldsymbol{A}_{11} & -\boldsymbol{L} \\ \boldsymbol{O} & \boldsymbol{F}_2 & -\boldsymbol{A}_{21} & -\boldsymbol{A}_{22} \\ -\boldsymbol{A}_{11}^T & -\boldsymbol{A}_{21}^T & -\boldsymbol{E}_1 & \boldsymbol{O} \\ -\boldsymbol{L}^T & -\boldsymbol{A}_{22}^T & \boldsymbol{O} & -\boldsymbol{E}_2 \end{pmatrix} \end{array}
\tag{12}
$$

$_{358}$ where, in addition to (8), $\begin{pmatrix} \boldsymbol{F}_1 & \\ & \boldsymbol{F}_2 \end{pmatrix} = \boldsymbol{PFP}^T$ and $\begin{pmatrix} \boldsymbol{E}_1 & \\ & \boldsymbol{E}_2 \end{pmatrix} = \boldsymbol{R}^T\boldsymbol{ER}$ are defined. In what follows the block

$_{359}$ four-by-four Jacobian matrix on the right will be the focus. Any variables involved in calculations with the permuted

$_{360}$ Jacobian which need to be in the original (un-permuted) order can easily be recovered using the matrices $\boldsymbol{P}$ and $\boldsymbol{R}$

$_{361}$ and their transposes. Therefore, the primary system to be considered is

$$
\begin{pmatrix} \boldsymbol{F}_1 & \boldsymbol{O} & -\boldsymbol{A}_{11} & -\boldsymbol{L} \\ \boldsymbol{O} & \boldsymbol{F}_2 & -\boldsymbol{A}_{21} & -\boldsymbol{A}_{22} \\ -\boldsymbol{A}_{11}^T & -\boldsymbol{A}_{21}^T & -\boldsymbol{E}_1 & \boldsymbol{O} \\ -\boldsymbol{L}^T & -\boldsymbol{A}_{22}^T & \boldsymbol{O} & -\boldsymbol{E}_2 \end{pmatrix} \begin{pmatrix} \boldsymbol{\phi}_1 \\ \boldsymbol{\phi}_2 \\ \boldsymbol{\phi}_3 \\ \boldsymbol{\phi}_4 \end{pmatrix} = \begin{pmatrix} \boldsymbol{w} \\ \boldsymbol{x} \\ \boldsymbol{y} \\ \boldsymbol{z} \end{pmatrix}.
\tag{13}
$$

$_{363}$ The system (13) can be seen as a rearrangement of (5) if $\boldsymbol{w}, \boldsymbol{x}, \boldsymbol{y}$ and $\boldsymbol{z}$ are defined to match the (appropriately

$_{364}$ permuted) right-hand-side of (5). In that case the solutions to the system, $\boldsymbol{\phi}_1, \boldsymbol{\phi}_2, \boldsymbol{\phi}_3, \boldsymbol{\phi}_4$ have important interpreta-

$_{365}$ tions: the vector $\boldsymbol{\phi}_1$ represents the Newton corrections to the flows for the pipes in the external and internal forests,

$_{366}$ $\boldsymbol{\phi}_4$ represents the Newton corrections to the heads at the nodes of the external and internal forests, $\boldsymbol{\phi}_2$ represents

$_{367}$ the Newton corrections to the flows in the topological minor superlinks in the core and $\boldsymbol{\phi}_3$ represents the Newton

$_{368}$ corrections to heads at the nodes of the topological minor (the supernodes). The form and structure of the nonlinear

$_{369}$ subsystem which models the behaviour of the topological minor heads and flows corrections provides some interesting

$_{370}$ insights and it is now presented. This subsystem is characterized in Lemma 1.

$_{371}$ **Lemma 1** *The vectors* $\boldsymbol{\phi}_2$ *and* $\boldsymbol{\phi}_3$ *of (13) satisfy*

$$
\begin{array}{c} \\ n_2 \\ n_3 \end{array}
\begin{array}{cc} n_2 & n_3 \\
\begin{pmatrix} \boldsymbol{B}_{11} & -\boldsymbol{B}_{12} \\ -\boldsymbol{B}_{12}^T & -\boldsymbol{B}_{22} \end{pmatrix} \end{array}
\begin{pmatrix} \boldsymbol{\phi}_2 \\ \boldsymbol{\phi}_3 \end{pmatrix} = \begin{pmatrix} \boldsymbol{u}_1 \\ \boldsymbol{u}_2 \end{pmatrix}
\tag{14}
$$

where

$$W = E_2 + L^T F_1^{-1} L \in \mathbb{R}^{n_1 \times n_1} \tag{15}$$

$$B_{11} = F_2 + A_{22} W^{-1} A_{22}^T \in \mathbb{R}^{n_2 \times n_2} \tag{16}$$

$$B_{12} = A_{21} - A_{22} W^{-1} L^T F_1^{-1} A_{11} \in \mathbb{R}^{n_2 \times n_3} \tag{17}$$

$$B_{22} = E_1 + A_{11}^T L^{-T} E_2 W^{-1} L^T F_1^{-1} A_{11} \in \mathbb{R}^{n_3 \times n_3} \tag{18}$$

$$u_1 = x - A_{22} W^{-1} \left[z + L^T F_1^{-1} w \right] \in \mathbb{R}^{n_2} \tag{19}$$

$$u_2 = y + A_{11}^T L^{-T} (E_2 W^{-1} (z + L^T F_1^{-1} w) - z) \in \mathbb{R}^{n_3} \tag{20}$$

Proof. See the Appendices. ∎

The matrix

$$B = \begin{pmatrix} B_{11} & -B_{12} \\ -B_{12}^T & -B_{22} \end{pmatrix} \tag{21}$$

is the topological minor's Jacobian, the equivalent of the full system's Jacobian in (3). However, it differs from the full Jacobian in an important respect. The matrix B_{12} in its $(1,2)$ block is not necessarily an ANIM in the case of a PDM problem. In fact, B_{12} can be considered to have two components. From (17) and (15) it follows that

$$B_{12} = A_{21} - A_{22} W^{-1} L^T F_1^{-1} A_{11}$$

$$= A_{21} - A_{22} W^{-1} \left(L^T F_1^{-1} L \right) L^{-1} A_{11}$$

$$= A_{21} - A_{22} W^{-1} \left(W - E_2 \right) L^{-1} A_{11} \text{ , so}$$

$$B_{12} = \left(A_{21} - A_{22} L^{-1} A_{11} \right) + A_{22} W^{-1} E_2 L^{-1} A_{11} \tag{22}$$

and so its first component, $A_{21} - A_{22} L^{-1} A_{11}$, is fixed and is the ANIM for the network's topological minor but there is also a second component which depends on the heads. The matrix B for the example network shown in Fig. 1 and which is given in (29) illustrates this point. The ANIM for that network before permutation is shown in Table 1 and after permutation in Table 5.

A number of other observations can be made about B and its components. The matrix, $-W$ is easily seen to be the Schur complement of the matrix

$$\begin{pmatrix} F_1 & -L \\ -L^T & -E_2 \end{pmatrix}$$

and its inverse is the main component of the matrix of PDM first-order sensitivities (Piller et al. 2016) of the (internal and external) forest heads to changes in the (internal and external) forest node demands, relative roughnesses, diameters and resistance factors. Here F_1 is the diagonal matrix of (> 0 for the Darcy-Weisbach head loss model) derivatives

of the (internal and external) forest head losses, $\boldsymbol{E}_2$ is the diagonal matrix of the (≥ 0) derivatives of the forest node consumption functions and $\boldsymbol{L}$ is the ANIM for the forest. The matrix $\boldsymbol{W}$ is symmetric, positive definite because it is the sum of a diagonal non-negative matrix and the product $\boldsymbol{L}^T \boldsymbol{F}_1^{-1} \boldsymbol{L}$ which is such that, for any non-vanishing $\boldsymbol{x} \in \mathbb{R}^{n_1}$, $\boldsymbol{x}^T \boldsymbol{L}^T \boldsymbol{F}_1^{-1} \boldsymbol{L} \boldsymbol{x} = \left\| \boldsymbol{F}_1^{-\frac{1}{2}} \boldsymbol{L} \boldsymbol{x} \right\|_2^2 > 0$. From the sensitivity matrix formulae given in Piller et al. (2016) it follows that the quantity $\boldsymbol{F}_1^{-1} \boldsymbol{L} \boldsymbol{W}^{-1}$ is proportional to the first-order change in inflow from a tree node into a tree link.

It is shown in what follows that the matrices $\boldsymbol{B}_{11}$ and $\boldsymbol{B}_{22}$ are diagonal. The matrix $\boldsymbol{B}_{11}$ is made up of two terms: the first, $\boldsymbol{F}_2$, which has the head loss derivatives due to the network internal cotree links (Deuerlein et al. 2016) and the second, $\boldsymbol{A}_{22} \boldsymbol{W}^{-1} \boldsymbol{A}_{22}^T$, which measures the contribution to the head loss derivatives attributable to the internal and external forest. The matrix $\boldsymbol{B}_{22}$, which gives the derivatives of the supernode consumption functions, also has two components. The first, $\boldsymbol{E}_1$, has the contribution to the derivatives of the consumption function due to the supernode itself, while the second term, $\boldsymbol{A}_{11}^T \boldsymbol{L}^{-T} \boldsymbol{E}_2 \boldsymbol{W}^{-1} \boldsymbol{L}^T \boldsymbol{F}_1^{-1} \boldsymbol{A}_{11}$, characterizes the contribution to the derivatives of the consumption functions at the supernodes made by the external and internal forests.

Denote

$$\boldsymbol{S}_B \stackrel{\text{def}}{=} \boldsymbol{B}_{22} + \boldsymbol{B}_{12}^T \boldsymbol{B}_{11}^{-1} \boldsymbol{B}_{12} \in \mathbb{R}^{n_3 \times n_3}. \tag{23}$$

The matrix $-\boldsymbol{S}_B$ is the Schur complement of the matrix, $\boldsymbol{B}$, in (21) and, once again, its inverse is the main component in the matrix of PDM first-order sensitivities of the heads in the topological minor to changes in the demands, relative roughnesses, diameters and resistance factors.

The two lemmas that follow give the solution $\boldsymbol{\phi}^T = (\boldsymbol{\phi}_1^T, \boldsymbol{\phi}_2^T, \boldsymbol{\phi}_3^T, \boldsymbol{\phi}_4^T)^T$ of the full system (13) in terms of the topological minor system.

Lemma 2 *With the definitions in Lemma 1, provided all the inverses exist,*

$$\boldsymbol{\phi}_3 = -\boldsymbol{S}_B^{-1}(\boldsymbol{u}_2 + \boldsymbol{B}_{12}^T \boldsymbol{B}_{11}^{-1} \boldsymbol{u}_1) \text{ and } \boldsymbol{\phi}_2 = \boldsymbol{B}_{11}^{-1}(\boldsymbol{u}_1 + \boldsymbol{B}_{12} \boldsymbol{\phi}_3). \tag{24}$$

Lemma 3 *With the definitions of Lemma 1 and Lemma 2,*

$$\boldsymbol{\phi}_4 = -\boldsymbol{W}^{-1} \left(\boldsymbol{L}^T \boldsymbol{F}_1^{-1}(\boldsymbol{w} + \boldsymbol{A}_{11} \boldsymbol{\phi}_3) + \boldsymbol{z} + \boldsymbol{A}_{22}^T \boldsymbol{\phi}_2 \right) \text{ and } \boldsymbol{\phi}_1 = -\boldsymbol{L}^{-T} \left(\boldsymbol{E}_2 \boldsymbol{\phi}_4 + \boldsymbol{z} + \boldsymbol{A}_{22}^T \boldsymbol{\phi}_2 \right).$$

The proofs of Lemma 2 and Lemma 3 follow immediately by substitution.

For completeness, it is worth mentioning that the submatrices in the system (14) for the case where only the FCPA

is used simplify, in view of the fact that $\boldsymbol{A}_{22} = \boldsymbol{O}$ in that case, to

$$\boldsymbol{W} = \boldsymbol{E}_2 + \boldsymbol{L}^T \boldsymbol{F}_1^{-1} \boldsymbol{L} \in \mathbb{R}^{n_1 \times n_1}, \quad \boldsymbol{B}_{11} = \boldsymbol{F}_2 \in \mathbb{R}^{n_2 \times n_2}, \quad \boldsymbol{B}_{12} = \boldsymbol{A}_{21} \in \mathbb{R}^{n_2 \times n_3},$$

$$\boldsymbol{B}_{22} = \boldsymbol{E}_1 + \boldsymbol{A}_{11}^T \boldsymbol{L}^{-T} \boldsymbol{E}_2 \boldsymbol{W}^{-1} \boldsymbol{L}^T \boldsymbol{F}_1^{-1} \boldsymbol{A}_{11} \in \mathbb{R}^{n_3 \times n_3},$$

$$\boldsymbol{u}_1 = \boldsymbol{x} \in \mathbb{R}^{n_2}, \quad \boldsymbol{u}_2 = \boldsymbol{y} + \boldsymbol{A}_{11}^T \boldsymbol{L}^{-T} (\boldsymbol{E}_2 \boldsymbol{W}^{-1} (\boldsymbol{z} + \boldsymbol{L}^T \boldsymbol{F}_1^{-1} \boldsymbol{w}) - \boldsymbol{z}) \in \mathbb{R}^{n_3}$$

For the case where the FCPA (and not the GMPA) is used in a DDM problem the Newton system for the steady-state heads and flows assumes the block lower triangular form, for some $\boldsymbol{w}^{(m)}$ and $\boldsymbol{x}^{(m)}$,

$$\begin{pmatrix} \boldsymbol{F}_1 & \boldsymbol{O} & -\boldsymbol{A}_{11} & -\boldsymbol{L} \\ \boldsymbol{O} & \boldsymbol{F}_2 & -\boldsymbol{A}_{21} & \\ -\boldsymbol{A}_{11}^T & -\boldsymbol{A}_{21}^T & & \\ -\boldsymbol{L}^T & & & \end{pmatrix} \begin{pmatrix} \boldsymbol{q}_1^{(m+1)} \\ \boldsymbol{q}_2^{(m+1)} \\ \boldsymbol{h}_3^{(m+1)} \\ \boldsymbol{h}_4^{(m+1)} \end{pmatrix} = \begin{pmatrix} \boldsymbol{w}^{(m)} \\ \boldsymbol{x}^{(m)} \\ \boldsymbol{d}_1 \\ \boldsymbol{d}_2 \end{pmatrix} \tag{25}$$

with $\boldsymbol{d}_1$ being the core demands and $\boldsymbol{d}_2$ the forest demands. The partitioning in (25) offers another formal proof of the well-known fact that when the GGA is applied to a DDM problem, the forest flows achieve their steady-state values after the first iteration. This is because the last block equation in (25) has the form $-\boldsymbol{L}^T \boldsymbol{q}_1^{(m+1)} = \boldsymbol{d}_2$, and so $\boldsymbol{q}_1^{(m+1)}$ is clearly independent of m. It is clear from the form of the Jacobian in (13) that the FCPA on its own cannot resolve the forest flows independently of the core flows when PDM is used. One of the main contributions of this paper is to extend the application of the FCPA to the case of PDM.

The topological minor system (14) provides insights into the connectivity and hydraulic behaviour of a WDS network. The superlinks and supernodes characterize the main elements of the network when the linear components (the internal and external forests, the heads and flows of which can be found by linear processes) are factored out. Dealing with the much smaller topological minor therefore presents an attractive option. The submatrix dimensions, n_p, n_j, n_1, n_2 and n_3, for the eight case study networks N_1 to N_8 used in Elhay et al. (2016) are shown in Columns 2-6 of Table 7. From these data it can be seen that in all cases the Schur complements of the topological minor's Jacobians have much smaller dimension (n_3) than the Schur complements of the full system's Jacobians (n_j). For example, the N_8 Schur complement has dimension $n_3 = 3,202$ while the full Jacobian Schur complement has dimension $n_j = 17,971$. Thus, where the topological minor can be used in place of the full Jacobian, significant savings can be realized.

The diagonality of the matrices $\boldsymbol{B}_{11}$ and $\boldsymbol{B}_{22}$ also confers significant computational efficiencies when dealing with the system (14): in particular the inversion of $\boldsymbol{B}_{11}$ becomes trivial. These properties are proved, and their implications discussed, next.

Properties of the matrices in the topological minor system and the Schur complements

The matrix $\boldsymbol{L}$ is block diagonal with lower triangular blocks and so $\boldsymbol{L}^T\boldsymbol{L}$ and $\boldsymbol{L}\boldsymbol{L}^T$ and their inverses are block diagonal with (generally) full diagonal blocks. Consequently, the matrix $\boldsymbol{W} = \boldsymbol{E}_2 + \boldsymbol{L}^T\boldsymbol{F}_1^{-1}\boldsymbol{L}$, and its inverse are block diagonal with (generally) full diagonal blocks. Using these properties it is possible to show that both of the topological minor matrices $\boldsymbol{B}_{11} = \boldsymbol{F}_2 + \boldsymbol{A}_{22}\boldsymbol{W}^{-1}\boldsymbol{A}_{22}^T$ and $\boldsymbol{B}_{22} = \boldsymbol{E}_1 + \boldsymbol{A}_{11}^T\boldsymbol{L}^{-T}\boldsymbol{E}_2\boldsymbol{W}^{-1}\boldsymbol{L}^T\boldsymbol{F}_1^{-1}\boldsymbol{A}_{11}$ are diagonal. This makes the inversion of $\boldsymbol{B}_{11}$ in (23) (24) trivial and adds to the efficiency of sparse matrix arithmetic with these matrices. The proofs of these computationally important properties are given in the Appendices.

As previously noted, the inverse, $\boldsymbol{S}_F^{-1}$, of the Schur complement of the full Jacobian $\boldsymbol{J}$ is a matrix which is central to the first-order sensitivity theory of WDSs. In view of the blocking in (12), the Schur complement of $\boldsymbol{J}$ can be written

$$
\begin{aligned}
\boldsymbol{S}_F &= \boldsymbol{E} + \boldsymbol{A}^T\boldsymbol{F}^{-1}\boldsymbol{A} \\[4pt]
&= \begin{pmatrix} \boldsymbol{E}_1 & \\ & \boldsymbol{E}_2 \end{pmatrix} + \begin{pmatrix} \boldsymbol{A}_{11}^T & \boldsymbol{A}_{21}^T \\ \boldsymbol{L}^T & \boldsymbol{A}_{22}^T \end{pmatrix} \begin{pmatrix} \boldsymbol{F}_1^{-1} & \\ & \boldsymbol{F}_2^{-1} \end{pmatrix} \begin{pmatrix} \boldsymbol{A}_{11} & \boldsymbol{L} \\ \boldsymbol{A}_{21} & \boldsymbol{A}_{22} \end{pmatrix} \\[4pt]
&= \begin{pmatrix} \boldsymbol{E}_1 + \boldsymbol{A}_{11}^T\boldsymbol{F}_1^{-1}\boldsymbol{A}_{11} + \boldsymbol{A}_{21}^T\boldsymbol{F}_2^{-1}\boldsymbol{A}_{21} & \boldsymbol{A}_{11}^T\boldsymbol{F}_1^{-1}\boldsymbol{L} + \boldsymbol{A}_{21}^T\boldsymbol{F}_2^{-1}\boldsymbol{A}_{22} \\ \boldsymbol{L}^T\boldsymbol{F}_1^{-1}\boldsymbol{A}_{11} + \boldsymbol{A}_{22}^T\boldsymbol{F}_2^{-1}\boldsymbol{A}_{21} & \boldsymbol{W} + \boldsymbol{A}_{22}^T\boldsymbol{F}_2^{-1}\boldsymbol{A}_{22} \end{pmatrix} \\[6pt]
&\overset{\text{def}}{=} \begin{array}{c} \\ n_3 \\ n_1 \end{array}\!\!\begin{pmatrix} \overset{\displaystyle n_3}{\boldsymbol{H}_{11}} & \overset{\displaystyle n_1}{\boldsymbol{H}_{12}} \\ \boldsymbol{H}_{12}^T & \boldsymbol{H}_{22} \end{pmatrix}.
\end{aligned}
\tag{26}
$$

The next result provides a way of computing the $(1,1)$ block of $\boldsymbol{S}_F^{-1}$ without computing the inverse of the whole matrix. The importance of the $(1,1)$ block will be discussed shortly.

Lemma 4 The $(1,1)$ block of $\boldsymbol{S}_F^{-1}$ is $\boldsymbol{S}_H^{-1} = \left(\boldsymbol{H}_{11} - \boldsymbol{H}_{12}\boldsymbol{H}_{22}^{-1}\boldsymbol{H}_{12}^T\right)^{-1}$

$$
\begin{pmatrix} \boldsymbol{H}_{11} & \boldsymbol{H}_{12} \\ \boldsymbol{H}_{12}^T & \boldsymbol{H}_{22} \end{pmatrix}^{-1} = \begin{pmatrix} \boldsymbol{S}_H^{-1} & \times \\ \times & \times \end{pmatrix}
\tag{27}
$$

provided the inverses exist.

So, the $(1,1)$ block of $\boldsymbol{S}_F^{-1}$ is itself the inverse of the Schur complement, $\boldsymbol{S}_H$, of the Jacobian's Schur complement blocked as in (26).

Proof. A simple calculation shows that if

$$
\begin{pmatrix} \boldsymbol{H}_{11} & \boldsymbol{H}_{12} \\ \boldsymbol{H}_{12}^T & \boldsymbol{H}_{22} \end{pmatrix} \begin{pmatrix} \boldsymbol{X} & \boldsymbol{Y} \\ \boldsymbol{Y}^T & \boldsymbol{Z} \end{pmatrix} = \boldsymbol{I}. \text{ then } \boldsymbol{X} = \left(\boldsymbol{H}_{11} - \boldsymbol{H}_{12}\boldsymbol{H}_{22}^{-1}\boldsymbol{H}_{12}^T\right)^{-1} = \boldsymbol{S}_H^{-1}.
$$

∎

The next result is one of the main contributions of this paper.

Lemma 5 *Provided all the inverses exist,*

$$\boldsymbol{S}_B = \boldsymbol{B}_{22} + \boldsymbol{B}_{12}^T \boldsymbol{B}_{11}^{-1} \boldsymbol{B}_{12} = \boldsymbol{H}_{11} - \boldsymbol{H}_{12} \boldsymbol{H}_{22}^{-1} \boldsymbol{H}_{12}^T = \boldsymbol{S}_H \tag{28}$$

The proof is given in the Appendices.

This lemma shows that $\boldsymbol{S}_H^{-1}$ is the inverse of the Schur complement of the topological minor system (14) . In other words, the $(1,1)$ block of the inverse of the Schur complement for the full Jacobian $\boldsymbol{S}_F = \boldsymbol{E} + \boldsymbol{A}^T \boldsymbol{F}^{-1} \boldsymbol{A}$ is the inverse of the Schur complement of the topological minor system $\boldsymbol{S}_B = \boldsymbol{B}_{22} + \boldsymbol{B}_{12}^T \boldsymbol{B}_{11}^{-1} \boldsymbol{B}_{12}$. The expression for $\boldsymbol{S}_B$ is particularly convenient computationally because, as has been shown, both $\boldsymbol{B}_{11}$ and $\boldsymbol{B}_{22}$ are diagonal. But more importantly, the behaviour of the system which is of most interest is condensed into the topological minor and this allows the analysis to be focused on a much smaller network. The time savings which follow from not having to invert a large Schur complement and instead using the inverse of the smaller topological minor's Schur complement may mean the difference between an infeasible and a practical calculation in the sensitivity analysis of large networks. The matrix $\boldsymbol{S}_B^{-1}$ for the illustrative network shown in Fig. 1 is given in (30).

Efficient calculation of the diagonal matrices $\boldsymbol{B}_{11}$ and $\boldsymbol{B}_{22}$

The very special structural properties of the matrices in the topological minor system can be exploited to reduce the computational burden involved in the analysis of the systems. In view of the fact that the matrix $\boldsymbol{B}_{11} = \boldsymbol{F}_2 + \boldsymbol{A}_{22} \boldsymbol{W}^{-1} \boldsymbol{A}_{22}^T$, is diagonal, only the diagonal elements of the second term $\boldsymbol{e}_j^T \boldsymbol{A}_{22} \boldsymbol{W}^{-1} \boldsymbol{A}_{22}^T \boldsymbol{e}_j, \quad j = 1, 2, \ldots, n_2,$ where $\boldsymbol{e}_j \in \mathbb{R}^{n_2}$ is the j-th column of an identity, need be computed. The pipes in the core are represented in the submatrix $(\boldsymbol{A}_{21} \quad \boldsymbol{A}_{22})$. The nodes of the core are represented in $\boldsymbol{A}_{21}$ and nodes of the internal forest which connect to pipes in the core are represented in $\boldsymbol{A}_{22}$. So any row of $\boldsymbol{A}_{22}$ can either be all zero or else have a single nonzero which is ± 1. Consequently, $\boldsymbol{e}_j^T \boldsymbol{A}_{22} = \sigma \hat{\boldsymbol{e}}_i^T$ for some i, where $\hat{\boldsymbol{e}}_i \in \mathbb{R}^{n_1}$ is i-th column of an identity and $\sigma \in \{-1, 0, 1\}$. Thus, it is only necessary to compute the diagonal terms $\hat{\boldsymbol{e}}_i^T \boldsymbol{W}^{-1} \hat{\boldsymbol{e}}$ for those cases where σ is not zero. As a first step, the following scheme can be used.

Suppose that the matrix $\boldsymbol{L}$ has b lower triangular blocks (some may be 1×1 blocks, of course) with the j-th block having dimension m_j and row and column indices in the ordered set $\boldsymbol{s}_j = \{s_1, s_2, \ldots, s_{m_j}\}$. Then, $\sum_{j=1}^{b} m_j = n_1$. Denote by $\boldsymbol{X}(\boldsymbol{s}_j, \boldsymbol{s}_j)$ the submatrix of $\boldsymbol{X}$ made up of the rows and columns indexed in $\boldsymbol{s}_j$, with a similar notation for vectors. The following scheme computes the diagonal elements of $\boldsymbol{B}_{11}$ economically.

(a) For each $j = 1, 2, \ldots, b$:

(i) compute the j-th $m_j \times m_j$ block of $\boldsymbol{W}$ as $\boldsymbol{W}(\boldsymbol{s}_j, \boldsymbol{s}_j) = \boldsymbol{E}_2(\boldsymbol{s}_j, \boldsymbol{s}_j) + \boldsymbol{L}(\boldsymbol{s}_j, \boldsymbol{s}_j)^T \boldsymbol{F}_1^{-1}(\boldsymbol{s}_j, \boldsymbol{s}_j) \boldsymbol{L}(\boldsymbol{s}_j, \boldsymbol{s}_j).$

(ii) Solve the system $\boldsymbol{W}(\boldsymbol{s}_j, \boldsymbol{s}_j)\boldsymbol{x}_j = \boldsymbol{e}(\boldsymbol{s}_j)$, $(\boldsymbol{e}(\boldsymbol{s}_j) \in \mathbb{R}^{n_1}$ is the j-th unit vector). This computes the vector $\boldsymbol{x}_j = \boldsymbol{W}^{-1}\boldsymbol{e}_j$.

(iii) The jth component of $\boldsymbol{x}_j$ is the required diagonal term of $\boldsymbol{B}_{11}$.

The diagonal matrix $\boldsymbol{A}_{22}\boldsymbol{W}^{-1}\boldsymbol{A}_{22}^T$ is non-negative definite but even if its j-th diagonal element vanishes because the j-th row of $\boldsymbol{A}_{22}$ is zero, $\boldsymbol{B}_{11}$ is still symmetric positive definite because of $\boldsymbol{F}_2$.

The same block inverses of $\boldsymbol{W}^{-1}$ that are used in the computation of $\boldsymbol{B}_{11}$ can be used in the computation of the expression $\boldsymbol{B}_{22} = \boldsymbol{E}_1 + \boldsymbol{A}_{11}^T\boldsymbol{L}^{-T}\boldsymbol{E}_2\boldsymbol{W}^{-1}\boldsymbol{L}^T\boldsymbol{F}_1^{-1}\boldsymbol{A}_{11}$. The triangular blocks of $\boldsymbol{L}$ and its transpose mean that those terms require only a forward- or back-substitution thereby making the computation of $\boldsymbol{B}_{22}$ quite economical. The blocks on the diagonal of $\boldsymbol{W}^{-1}$ are decoupled from one another. Because of this, parallel or distributed computing with $\boldsymbol{W}^{-1}$ can be done very efficiently, a significant advantage when dealing with very large networks. Fig. 5 shows the frequency distribution of block sizes for the largest ($n_p = 19,647$) case study network used in this paper. The matrix $\boldsymbol{W}^{-1}$ has dimension $14,769$ but most of the $5,292$ blocks have quite modest dimension suggesting that exploiting the block diagonal nature of $\boldsymbol{W}^{-1}$ will be very advantageous.

Further significant computational savings may be available in analysing a network such as N_8. The steady-state PDM flows and heads for N_8 (with all demands amplified by a factor of 5 to make it a true PDM problem) were computed. Of the $15,332$ nodes with positive demands only $3,119$ deliver less than the required demand (i.e. are in the so-called partial delivery mode) while $12,213$ deliver the required demand. In a case such as this, the block calculations described above can be simplified for all the blocks which represent nodes that are not in a PDM state. Thus, there are then the following simplifications for those blocks: (i) the matrix $\boldsymbol{W}$ simplifies to $\boldsymbol{W} = \boldsymbol{L}^T\boldsymbol{F}_1^{-1}\boldsymbol{L}$ and, (ii) recalling (22), $\boldsymbol{B}_{12} = \boldsymbol{A}_{21} - \boldsymbol{A}_{22}\boldsymbol{L}^{-1}\boldsymbol{A}_{11}$ and can be precomputed before iterations start. In addition, those parts of $\boldsymbol{\phi}_1$ (which represents the forest flows) and $\boldsymbol{\phi}_4$ (which represents the forest heads) which correspond to blocks that are not in a PDM state can be handled as a DDM case would be. For networks such as this these savings can be important.

Which of $\boldsymbol{S}_B$ or $\boldsymbol{S}_H$ should be used in calculation?

It is natural to ask which of the equivalent expressions, $\boldsymbol{S}_B$, or $\boldsymbol{S}_H$ in (28) is preferable in practice since they produce the same matrix result. The computation time for many sparse matrix calculations such as matrix inversion is roughly proportional to the number of nonzeros in the matrix. On the face of it, inverting the matrices $\boldsymbol{B}_{11}$ and $\boldsymbol{H}_{22}$ in $\boldsymbol{S}_B$ and $\boldsymbol{S}_H$, respectively, present the biggest computational burdens. The relevant facts here are that (i) $\boldsymbol{B}_{11}$ is diagonal and so computing $\boldsymbol{B}_{11}^{-1}\boldsymbol{B}_{12}$ is no more than a row scaling of $\boldsymbol{B}_{12}$, but the matrix $\boldsymbol{H}_{22} \in \mathbb{R}^{n_1 \times n_1}$ is not, in general, diagonal and (ii) using the case study networks considered in this paper as a guide suggests that the matrices $\boldsymbol{H}_{22}$ usually have many more nonzeros than the corresponding matrices $\boldsymbol{B}_{11}$. Table 7 shows, for the eight

case study networks, the number of pipes n_p, the number of nodes n_j, the submatrix dimension parameters n_1, n_2 and n_3, together with the number of nonzeros in $\boldsymbol{B}_{11}$, $\boldsymbol{H}_{22}$ and the ratio of those two numbers as a percentage. In view of the much greater number of nonzeros in $\boldsymbol{H}_{22}$ for all cases and the fact that $\boldsymbol{H}_{22}$ is not diagonal, implying a greater computational burden in the inversion, the expression for $\boldsymbol{S}_B$ must be preferred. The cases of Networks 5 and 6 are particularly persuasive since there $\boldsymbol{B}_{11}$ has 3% or less of the number of nonzeros in $\boldsymbol{H}_{22}$.

AN EXAMPLE NETWORK

Example 1 In this section the partitioning of the network shown in Fig. 1 is discussed in more detail and the key matrices in the topological minor are displayed.

Table 1 shows the network's ANIM before any partitioning. The internal forest has been chosen to include nodes 3, 4, 5, 6, 7 and 8 and pipes 2, 3, 4, 5, 6 and 7. The topological minor of this network is shown in Fig. 2 (a) and the corresponding internal and external forest component is shown in Fig. 2 (b) with the internal tree chords, 1, 8, 9, 10, shown as dotted lines. Thus, pipes 2, 3 are internal tree branches and pipes 11 and 13 are external tree branches. These four pipes are represented by the first 4×4 block shown in the matrix $\boldsymbol{L}$ in Table 5. Note that node 4 has index 4 at start but after the external forest has been partitioned, it has index 2 and so qualifies for the internal forest. For this case $n_p = 13$, $n_j = 11$, $n_1 = 9$, $n_2 = 4$ and $n_3 = 2$. Table 5 shows the ANIM after FCPA, GMPA and Schilders factoring have all been applied. The matrix $\boldsymbol{L}$ in this case has 3 diagonal blocks which are lower triangular and which have dimensions 4×4, 1×1 and 4×4. The steady-state flows, heads, nodal deliveries, demands and deliveries as percentages of demands are shown in Table 6. To compute the topological minor, the matrices $\boldsymbol{F}_1$, $\boldsymbol{F}_2$, $\boldsymbol{E}_1$ and $\boldsymbol{E}_2$ of (12) are found by applying the permutations $\boldsymbol{P}$ and $\boldsymbol{R}$ to the Jacobian (3) and together with $\boldsymbol{L}$, which is the top-right block of the matrix shown in Table 5, are used to compute $\boldsymbol{W} = \boldsymbol{E}_2 + \boldsymbol{L}^T \boldsymbol{F}_1^{-1} \boldsymbol{L}$ and hence $\boldsymbol{B}_{11}$, $\boldsymbol{B}_{12}$ and $\boldsymbol{B}_{22}$ using (16) to (18). The resulting topological minor matrix $\boldsymbol{B}$ of (21) is then

$$
\boldsymbol{B} = \begin{pmatrix} \boldsymbol{B}_{11} & \boldsymbol{B}_{12} \\ \boldsymbol{B}_{12}^T & \boldsymbol{B}_{22} \end{pmatrix}
$$

$$
= \left(\begin{array}{cccc|cc}
308.2942 & 0 & 0 & 0 & 1 & 0 \\
0 & 126.4176 & 0 & 0 & -0.7476 & 1 \\
0 & 0 & 70.9984 & 0 & -0.3231 & 1 \\
0 & 0 & 0 & 85.0870 & -0.2860 & 1 \\
\hline
1 & -0.7476 & -0.3231 & -0.2860 & -0.0168 & 0 \\
0 & 1 & 1 & 1 & 0 & -0.0037
\end{array} \right) \tag{29}
$$

and $\boldsymbol{B}_{11}$, $\boldsymbol{B}_{22}$ are indeed diagonal. As noted earlier, $\boldsymbol{B}_{12}$ is not a true ANIM because some nodes are in a PDM state.

⁵⁶⁰ The form of the partitioned ANIM matrix in Table 5 illustrates the three block types which are possible on the

⁵⁶¹ block diagonal of $\boldsymbol{L}$: (i) a generally full lower triangular block, (ii) a diagonal block (in this case of dimension 1×1)

⁵⁶² and (iii) a lower bidiagonal block. The first block in $\boldsymbol{W}$ represents the union of two trees: one made up of the internal

⁵⁶³ forest pipes 2 and 3 and the other made up of the external forest pipes 11 and 13. Similarly, the last block in $\boldsymbol{W}$

⁵⁶⁴ represents the union of two trees: the internal forest pipes 5, 6 and 7 and external forest pipe 12. The corresponding

⁵⁶⁵ block structure of $\boldsymbol{W}^{-1}$ is clearly evident:

⁵⁶⁶
$$\boldsymbol{W}^{-1} = \begin{pmatrix} 47.4 & 29.3 & 26.8 & 26.8 & 0 & 0 & 0 & 0 & 0 \\ 29.3 & 55.3 & 50.6 & 50.6 & 0 & 0 & 0 & 0 & 0 \\ 26.8 & 50.6 & 69.8 & 46.3 & 0 & 0 & 0 & 0 & 0 \\ 26.8 & 50.6 & 46.3 & 69.8 & 0 & 0 & 0 & 0 & 0 \\ 0 & 0 & 0 & 0 & 67.3 & 0 & 0 & 0 & 0 \\ 0 & 0 & 0 & 0 & 0 & 47.2 & 30.8 & 25.3 & 23.2 \\ 0 & 0 & 0 & 0 & 0 & 30.8 & 57.2 & 47.0 & 43.1 \\ 0 & 0 & 0 & 0 & 0 & 25.3 & 47.0 & 64.3 & 58.9 \\ 0 & 0 & 0 & 0 & 0 & 23.2 & 43.1 & 58.9 & 77.2 \end{pmatrix}$$

⁵⁶⁷ Note that even though the last block of $\boldsymbol{E}_2 + \boldsymbol{L}^T \boldsymbol{F}_1^{-1} \boldsymbol{L}$ is tridiagonal, its inverse is generally full.

⁵⁶⁸ The matrix $\boldsymbol{S}_B^{-1}$ is, in accordance with (28), precisely the top-left block of $\boldsymbol{S}_F^{-1}$.

⁵⁶⁹
$$\boldsymbol{S}_F^{-1} = \begin{pmatrix} 45.9586 & 16.9873 & \\ 16.9873 & 33.0132 & \times \\ & \times & \end{pmatrix} = \begin{pmatrix} \boldsymbol{S}_B^{-1} & \times \\ \times & \times \end{pmatrix} \tag{30}$$

⁵⁷⁰ and $-\boldsymbol{S}_B^{-1}$ is the main component of the matrix of first-order sensitivities of the heads and flows at the supernodes,

⁵⁷¹ 1 and 2, to changes in the demands, relative roughnesses, diameters and resistance factors at those nodes. The full

⁵⁷² matrix of the first-order sensitivities of the heads, h_i, to demands, d_i is shown in Table 8. Note that, unlike the

⁵⁷³ DDM case, this PDM sensitivity matrix is not symmetric. The top-left 2×2 block of this matrix is the heads to

⁵⁷⁴ demands sensitivity matrix for the topological minor. It could have been computed much more economically by right-

⁵⁷⁵ multiplying the 2×2 block shown in (30) by a 2×2 diagonal matrix which has the d-derivatives of the consumption

⁵⁷⁶ functions for nodes 1 and 2 (see Piller et al. (2016) for explicit formulae to compute these sensitivity matrices from

⁵⁷⁷ $-\boldsymbol{S}_B^{-1}$ and see Deuerlein et al. (2017) for a discussion of DDM sensitivity matrices). There is no reason that the heads

⁵⁷⁸ of the nodes in the topological minor should be the most sensitive in the network – reducing the diameter of a pipe

⁵⁷⁹ can increase the sensitivity of a nearby node to arbitarily high levels. But the nodes of the topological minor are, as

⁵⁸⁰ explained earlier, the most important.

□

Example 2 The public domain Balerma network which was used in Reca & Martinez (2006) is a convincing example of a real life network in which the topological minor has significantly smaller dimension that of the full system. The full network had $n_p = 454$ pipes, $n_j = 443$ nodes and $n_f = 4$ sources. The full network is displayed in Fig. 6.

The supergraph matrix $\boldsymbol{A}_{21}$ for this network has dimension 27×16 and the (internal and external) forest has 427 elements. Fig. 7 Shows the network core after the FCPA has been applied and Fig. 8 shows the supergraph. The external forest is shown in Fig. 9.

□

APPLICATIONS OF THE PARTITIONING

The matrix $\boldsymbol{S}_B$ has application in several problems. As one example, the matrix which measures the first-order sensitivity of the PDM steady-state heads in a network to changes in the demands is $\boldsymbol{S}_F^{-1}\boldsymbol{T}$, $\boldsymbol{T}$ a diagonal matrix. Thus, it is the inverse of the Schur complement of $\boldsymbol{J}$ with its columns scaled. For large networks it may be prohibitively time consuming to invert such a large matrix. On the other hand, inverting the Schur complement, $\boldsymbol{S}_B$, of the much smaller topological minor matrix for the same network may well be practical and, since the most important aspects of the network's behaviour are encapsulated in the topological minor, this may be of more value. It is important to note in the context of sensitivity analysis, that the inverse of the Schur complement of the Jacobian figures in the expressions for the sensitivities of the steady-state heads and flows with respect to demands, resistance factors, roughnesses and pipe diameters. These remarks apply equally to DDM problems albeit with simplified formulae.

The inverse of the Jacobian's Schur complement also plays a central role in the calibration problem where, for example, the demands in a network are to be determined. In that case the demands at the topological minor nodes might be those most likely to be required since they influence network behaviour more strongly than other nodes. Once again, working with the smaller topological minor Schur complement will be more efficient.

In Elhay et al. (2016) a technique for solving PDM WDS problems by using a weighted least squares Gauss-Newton iteration was presented. Indicative tests suggest that using the partitioned solution scheme of (13) and exploiting the block structure of the matrix $\boldsymbol{W}$ and the diagonality of $\boldsymbol{B}_{11}$ and $\boldsymbol{B}_{22}$ to compute the Gauss-Newton descent direction leads to shorter execution times. Importantly, the independence of the blocks on the diagonal of $\boldsymbol{W}^{-1}$ means that each block can be treated on its own and that the simpler DDM formulae can be used where the nodes in a block are not in a PDM state.

CONCLUSIONS

In this paper the permutations used in (i) the FCPA which separate a network's external forest from its core,

⁶¹³ and (ii) the GMPA which separates a network core's internal forest from the rest of the core, and (iii) the Schilders

⁶¹⁴ permutations are put into a unified framework. Using this framework, the FCPA and the GMPA schemes for DDM

⁶¹⁵ problems have been extended to deal with PDM problems. All the PDM results in this paper are applicable to DDM

⁶¹⁶ problems by applying the appropriate simplifications.

⁶¹⁷   The Jacobian for the PDM topological minor has been derived and important structural properties of matrices

⁶¹⁸ involved in the topological minor have been established and formally proved. These include the diagonality of the

⁶¹⁹ matrices $\boldsymbol{B}_{11}$ and $\boldsymbol{B}_{22}$ and the block diagonal structure of the matrix $\boldsymbol{W}$. It is also shown that for an example network

⁶²⁰ with about 20,000 pipes the matrix $\boldsymbol{W}$ has many small blocks, a property which can be exploited to economize on

⁶²¹ computation, especially in a parallel or distributed computing environment.

⁶²²   It is shown that, $\boldsymbol{S}_B^{-1}$, the inverse of the Schur complement for the Jacobian of the topological minor, is precisely

⁶²³ the $(1,1)$ block of, $\boldsymbol{S}_F^{-1}$, the inverse of the Schur complement for the Jacobian of the full system. The matrix $\boldsymbol{S}_B^{-1}$ is

⁶²⁴ central to the study of first order sensitivities of heads and flows to changes in system demands, resistance factors,

⁶²⁵ roughnesses, relative roughnesses, and diameters. Given the significant computational cost of inverting $\boldsymbol{S}_F$ for a

⁶²⁶ large system, the possibility of computing only its $(1,1)$ block, $\boldsymbol{S}_B^{-1}$, is both attractive and helpful since in many

⁶²⁷ cases the topological minor encapsulates the most important information about a network. Schemes for the efficient

⁶²⁸ calculation of the matrices $\boldsymbol{B}_{11}$, $\boldsymbol{B}_{22}$ and $\boldsymbol{W}^{-1}$ and working with the topological minor subsystems are also given.

⁶²⁹ The partitioning technique and the matrix properties in this paper are illustrated with a small example network. The

⁶³⁰ relevance of these results to some important applications in water distribution analysis are briefly described.

⁶³¹   A useful contribution to the field would be the application of the partitioning technique to assess the resilience of

⁶³² large networks with pressure deficiencies that result from critical events.

⁶³³

⁶³⁸ References

⁶³⁹ Birkhoff, G. (1963), 'A variational principle for nonlinear networks', *Q. Appl. Math.* **21**(2), 160–162.

⁶⁴⁰ Boccaletti, S., Latora, V., Morenod, Y., Chavezf, M. & Hwanga, D.-U. (2006), 'Complex networks. structure and

⁶⁴¹   dynamics', *Physics Reports* **424**, 175–308.

Chiplunkar, A., Mehndiratta, S. & Khanna, P. (1990), 'Analysis of looped water distribution networks.', *Environmental Software* **5**(4), 202–206.

Crous, P., van Zyl, J. & Roodt, Y. (2012), 'The potential of graphical processing units to solve hydraulic network equations', *J. of Hydroinformatics* **14**(3), 603–612.

Deuerlein, J. (2006), Efficient supply network management based on linear graph theory, *in* 'Water Distribution Systems Analysis Symposium 2006', pp. 1–18.

Deuerlein, J. (2008), 'Decomposition model of a general water supply network graph', *J. Hydraul. Eng.* **134**(6), 822–832.

Deuerlein, J., Elhay, S. & Simpson, A. (2016), 'Fast graph matrix partitioning algorithm for solving the water distribution system equations', *J. Water Resour. Plann. Manage.* **142**(1). DOI: 10.1061/(ASCE)WR.1943-5452.0000561, 04015037.

Deuerlein, J., Piller, O., Elhay, S. & Simpson, A. (2017), Sensitivity analysis of topological subgraph of water distribution networks, *in* 'WDSA 2016: 18th Water Distribution Systems Analysis Conference, WDSA2016', Vol. 186, Universidad de los Andes, Cartagena, Columbia, pp. 252–260.

Deuerlein, J., Piller, O. & Montalvo, I. (2014), 'Improved real-time monitoring and control of water supply networks by use of graph decomposition', *Procedia Engineering* **89**, 12761281. 16th Water Distribution System Analysis Conference, WDSA2014 Urban Water Hydroinformatics and Strategic Planning.

Di Nardo, A., Di Natale, M., Giudicianni, C., Greco, R. & Santonastaso, G. (2016), 'Water supply network partitioning based on weighted spectral clustering', *Studies in Computational Intelligence: Complex Networks & Their Applications* **693**, 797–807.

Diao, K., Wang, Z., Burger, G., Chen, C., Rauch, W. & Zhou, Y. (2014), 'Speedup of water distribution simulation by domain decomposition.', *Environ. Model. Softw.* **52**, 253–263.

Diestel, R. (2010), *Graph Theory*, Vol. 173 of *Graduate texts in mathematics*, fourth edn, Springer-Verlag, Heidelberg.

Dolan, A. & Aldous, J. (1993), *Networks and algorithms: an introductory approach*, J. Wiley & Sons.

Elhay, S., Piller, O., Deuerlein, J. & Simpson, A. (2016), 'A robust, rapidly convergent method that solves the water distribution equations for pressure dependent models', *J. Water Resour. Plann. Manage.* **142**(2). DOI: 10.1061/(ASCE)WR.1943-5452.0000578.

Elhay, S., Simpson, A., Deuerlein, J., Alexander, B. & Schilders, W. (2014), 'A reformulated co-tree flows method competitive with the Global Gradient Algorithm for solving the water distribution system equations', *J. Water Resour. Plann. Manage.* **140**(12). DOI: 10.1061/(ASCE)WR.1943-5452.0000431.

Estrada, E. (2006), 'Network robustness to targeted attacks. the interplay of expansibility and degree distribution', *The European Physical Journal B-Condensed Matter and Complex Systems* .

Giustolisi, O. & Laucelli, D. (2011), 'Water distribution network pressure-driven analysis using the enhanced global gradient algorithm (egga)', *J. Water Resour. Plann. Manage.* **137**(11), 498–510.

Giustolisi, O., Savic, D., Laucelli, D. & Berardi, L. (2011), Testing linear solvers for WDN models, *in* 'Computing and Control for the Water Industry 2011', Urban Water Management: Challenges and Opportunities, Exeter. CD-ROM.

Guidolin, M., Savic, D. & Kapelan, Z. (2011), Computational performance analysis and improvement of the demand-driven hydraulic solver for the cwsnet library, *in* 'Computing and Control for the Water Industry 2011', Vol. 1 of *Urban Water Management: Challenges and Opportunities*, Exeter, pp. 45–50. CD-ROM.

Herrera, H., Canu, S., Karatzoglou, A., Prez-Garca, R. & Izquierdo, J. (2010), An approach to water supply clusters by semi-supervised learning, *in* 'Proceedings of International Environmental Modelling and Software Society'.

Lan, F., Lin, W. & Lansey, K. (2015), 'Scenario-based robust optimization of a water supply system under risk of facility failure.', *Environ. Model. Softw.* **67**, 160–172.

Laucelli, D., Berardi, L. & Giustolisi, O. (2012), 'Assessing climate change and asset deterioration impacts on water distribution networks: Demand-driven or pressure-driven network modeling?', *Environ. Model. Softw.* **37**, 206–216.

Mathworks, T. (2016), *MATLAB version 9.1.0.441655 (R2016b)*, Natick, Massachusetts.

Perelman, L. & Ostfeld, A. (2011), 'Topological clustering for water distribution systems analysis.', *Environ. Model. Softw.* **26**, 969–972.

Perelman, L. S., Allen, M., Preis, A., Iqbal, M. & Whittle, A. (2015), 'Automated sub-zoning of water distribution systems.', *Environ. Model.Softw.* **65**, 1–14.

Piller, O., Elhay, S., Deuerlein, J. & Simpson, A. (2016), 'Local sensitivity of pressure dependent modeling and demand dependent modeling steady-state solutions to variations in parameters', *J. Water Resour. Plann. Manage.* **142**(2). DOI: 10.1061/(ASCE)WR.1943-5452.0000729, 04016074.

Piller, O., Le Fichant, M. & van Zyl, J. (2012), Lessons learned from restructuring a hydraulic solver for parallel computing, Engineers Australia, Adelaide, South Australia, pp. 398–406. WDSA 2012: 14th Water Distribution Systems Analysis Conference.

Puust, R., Maddison, M. & Laanearu, J. (2011), Reviewing the effectiveness of gpu power when used for water network optimization problems, *in* 'Computing and Control for the Water Industry 2011', Urban Water Management: Challenges and Opportunities, Exeter. CD-ROM.

Reca, J. & Martinez, J. (2006), 'Genetic algorithms for the design of looped irrigation water distribution networks', *Water Resources Research* **42**(W05416). DOI: 10.1029/2005WR004383.

ResiWater (2017), 'Resiwater: Innovative secure sensor networks and model-based assessment tools for increased resilience of water infrastructures'. `http://www.resiwater.eu/project/`.

Schilders, W. (2009), 'Solution of indefinite linear systems using an LQ decomposition for the linear constraints', *Linear Algebra Appl.* **431**, 381–395.

Simpson, A., Elhay, S. & Alexander, B. (2014), 'Forest-core partitioning algorithm for speeding up the analysis of water distribution systems', *J. Water Resour. Plann. Manage.* **140**(4), 435–443. DOI: 10.1061/(ASCE)WR.1943-5452.0000336.

Todini, E. & Pilati, S. (1988), *A gradient algorithm for the analysis of pipe networks.*, John Wiley and Sons, London, pp. 1–20.

Tzatchkov, V., Alcocer-Yamanaka, V. & Rodriguez-Varela, J. (2006), Water distribution network sectorization projects in mexican cities along the border with usa, *in* 'In: Proc. of the 3rd International Symposium on Transboundary Water Management', Ciudad Real, Spain, pp. 1–13.

van Zyl, J., Savic, D. & Walters, G. (2006), 'Explicit integration method for extended-period simulation of water distribution systems', *J. Hydraulic. Eng.* **132**(4), 385–392.

Wu, Z. & Lee, I. (2011), Lessons for parallelizing linear equation solvers and water distribution analysis, *in* 'Computing and Control for the Water Industry 2011', Urban Water Management: Challenges and Opportunities, Exeter. CD-ROM.

Yazdani, A., Otoo, R. & Jeffrey, P. (2011), 'Resilience enhancing expansion strategies for water distribution systems: A network theory approach.', *Environ. Model. Softw.* **26**, 1574–1582.

Zecchin, A., Thum, P., Simpson, A. & Tischendorf, C. (2012), 'Steady-state behavior of large water distribution systems: Algebraic multigrid method for the fast solution of the linear step', *J. Water Resources Planning and Management* .

APPENDICES

PROOF OF LEMMA 1

The first and last block equations of (13) can be written as

$$\begin{pmatrix} \boldsymbol{F}_1 & -\boldsymbol{L} \\ -\boldsymbol{L}^T & -\boldsymbol{E}_2 \end{pmatrix} \begin{pmatrix} \boldsymbol{\phi}_1 \\ \boldsymbol{\phi}_4 \end{pmatrix} = \begin{pmatrix} \boldsymbol{w} + \boldsymbol{A}_{11}\boldsymbol{\phi}_3 \\ \boldsymbol{z} + \boldsymbol{A}_{22}^T\boldsymbol{\phi}_2 \end{pmatrix}.$$

Thus,

$$\begin{pmatrix} \boldsymbol{F}_1 & -\boldsymbol{L} \\ \boldsymbol{O} & -\boldsymbol{E}_2 - \boldsymbol{L}^T\boldsymbol{F}_1^{-1}\boldsymbol{L} \end{pmatrix} \begin{pmatrix} \boldsymbol{\phi}_1 \\ \boldsymbol{\phi}_4 \end{pmatrix} = \begin{pmatrix} \boldsymbol{I} & \boldsymbol{O} \\ \boldsymbol{L}^T\boldsymbol{F}_1^{-1} & \boldsymbol{I} \end{pmatrix} \begin{pmatrix} \boldsymbol{w} + \boldsymbol{A}_{11}\boldsymbol{\phi}_3 \\ \boldsymbol{z} + \boldsymbol{A}_{22}^T\boldsymbol{\phi}_2 \end{pmatrix}$$

and provided that $\boldsymbol{W} \overset{\text{def}}{=} \boldsymbol{E}_2 + \boldsymbol{L}^T\boldsymbol{F}_1^{-1}\boldsymbol{L}$ is invertible

$$\boldsymbol{\phi}_4 = \left[-\boldsymbol{W}^{-1}\boldsymbol{A}_{22}^T \right] \boldsymbol{\phi}_2 + \left[-\boldsymbol{W}^{-1}\boldsymbol{L}^T\boldsymbol{F}_1^{-1}\boldsymbol{A}_{11} \right] \boldsymbol{\phi}_3 - \boldsymbol{W}^{-1} \left[\boldsymbol{z} + \boldsymbol{L}^T\boldsymbol{F}_1^{-1}\boldsymbol{w} \right]. \tag{31}$$

From the fourth block equation

$$\boldsymbol{\phi}_1 = -\boldsymbol{L}^{-T} \left(\boldsymbol{E}_2\boldsymbol{\phi}_4 + \boldsymbol{z} + \boldsymbol{A}_{22}^T\boldsymbol{\phi}_2 \right)$$

or

$$\boldsymbol{\phi}_1 = \left[\boldsymbol{L}^{-T}(\boldsymbol{E}_2\boldsymbol{W}^{-1} - \boldsymbol{I})\boldsymbol{A}_{22}^T \right] \boldsymbol{\phi}_2 + \left[\boldsymbol{L}^{-T}\boldsymbol{E}_2\boldsymbol{W}^{-1}\boldsymbol{L}^T\boldsymbol{F}_1^{-1}\boldsymbol{A}_{11} \right] \boldsymbol{\phi}_3 + \left[\boldsymbol{L}^{-T}(\boldsymbol{E}_2\boldsymbol{W}^{-1}(\boldsymbol{z} + \boldsymbol{L}^T\boldsymbol{F}_1^{-1}\boldsymbol{w}) - \boldsymbol{z}) \right]. \tag{32}$$

The second and third block equations of (13) can be written

$$\boldsymbol{F}_2\boldsymbol{\phi}_2 - \boldsymbol{A}_{21}\boldsymbol{\phi}_3 - \boldsymbol{A}_{22}\boldsymbol{\phi}_4 \;=\; \boldsymbol{x} \tag{33}$$

$$-\boldsymbol{A}_{11}^T\boldsymbol{\phi}_1 - \boldsymbol{A}_{21}^T\boldsymbol{\phi}_2 - \boldsymbol{E}_1\boldsymbol{\phi}_3 \;=\; \boldsymbol{y} \tag{34}$$

Substituting the expressions for $\boldsymbol{\phi}_1, \boldsymbol{\phi}_4$ into these equations and collecting terms gives a system in the two unknowns $\boldsymbol{\phi}_2, \boldsymbol{\phi}_3$. Substituting the expression for $\boldsymbol{\phi}_4$ in (31) into (33) gives

$$\left[\boldsymbol{F}_2 + \boldsymbol{A}_{22}\boldsymbol{W}^{-1}\boldsymbol{A}_{22}^T \right] \boldsymbol{\phi}_2 - \left[\boldsymbol{A}_{21} - \boldsymbol{A}_{22}\boldsymbol{W}^{-1}\boldsymbol{L}^T\boldsymbol{F}_1^{-1}\boldsymbol{A}_{11} \right] \boldsymbol{\phi}_3 = \boldsymbol{x} - \boldsymbol{A}_{22}\boldsymbol{W}^{-1} \left[\boldsymbol{z} + \boldsymbol{L}^T\boldsymbol{F}_1^{-1}\boldsymbol{w} \right]. \tag{35}$$

Substituting the expression for $\boldsymbol{\phi}_1$ in (32) into (34) gives

$$
\begin{aligned}
-\left[\boldsymbol{A}_{21}^T + \boldsymbol{A}_{11}^T \boldsymbol{L}^{-T}(\boldsymbol{E}_2 \boldsymbol{W}^{-1} - \boldsymbol{I})\boldsymbol{A}_{22}^T\right] \boldsymbol{\phi}_2 & \\
+ \left[-\boldsymbol{E}_1 - \boldsymbol{A}_{11}^T \boldsymbol{L}^{-T} \boldsymbol{E}_2 \boldsymbol{W}^{-1} \boldsymbol{L}^T \boldsymbol{F}_1^{-1} \boldsymbol{A}_{11}\right] \boldsymbol{\phi}_3 & \\
= \boldsymbol{A}_{11}^T \boldsymbol{L}^{-T}(\boldsymbol{E}_2 \boldsymbol{W}^{-1}(\boldsymbol{z} + \boldsymbol{L}^T \boldsymbol{F}_1^{-1}\boldsymbol{w}) - \boldsymbol{z}) + \boldsymbol{y}. &
\end{aligned}
\tag{36}
$$

Lemma 6 *If $\boldsymbol{W} = \boldsymbol{E}_2 + \boldsymbol{L}^T \boldsymbol{F}_1^{-1}\boldsymbol{L}$, and $\boldsymbol{L}$ are both invertible, then $(\boldsymbol{A}_{21} - \boldsymbol{A}_{22}\boldsymbol{W}^{-1}\boldsymbol{L}^T \boldsymbol{F}_1^{-1}\boldsymbol{A}_{11})^T = \boldsymbol{A}_{21}^T + \boldsymbol{A}_{11}^T \boldsymbol{L}^{-T}(\boldsymbol{E}_2 \boldsymbol{W}^{-1} - \boldsymbol{I})\boldsymbol{A}_{22}^T$.*

Proof. $\boldsymbol{I} - \boldsymbol{W}^{-1}\boldsymbol{E}_2 = \boldsymbol{W}^{-1}(\boldsymbol{W} - \boldsymbol{E}_2) = \boldsymbol{W}^{-1}(\boldsymbol{L}^T \boldsymbol{F}_1^{-1}\boldsymbol{L})$ and so $\boldsymbol{W}^{-1}\boldsymbol{L}^T \boldsymbol{F}_1^{-1} = (\boldsymbol{I} - \boldsymbol{W}^{-1}\boldsymbol{E}_2)\boldsymbol{L}^{-1}$. Now, $\boldsymbol{W}$ is symmetric so $\boldsymbol{W}^{-T} = \boldsymbol{W}^{-1}$ and $(\boldsymbol{W}^{-1}\boldsymbol{L}^T \boldsymbol{F}_1^{-1})^T = \boldsymbol{L}^{-T}(\boldsymbol{I} - \boldsymbol{E}_2 \boldsymbol{W}^{-1})$ whence $-(\boldsymbol{A}_{22}\boldsymbol{W}^{-1}\boldsymbol{L}^T \boldsymbol{F}_1^{-1}\boldsymbol{A}_{11})^T = \boldsymbol{A}_{11}^T \boldsymbol{L}^{-T}(\boldsymbol{E}_2 \boldsymbol{W}^{-1} - \boldsymbol{I})\boldsymbol{A}_{22}^T$ from which the identity quickly follows. ∎

Thus, (36) can be rewritten as

$$
\begin{aligned}
-\left[\boldsymbol{A}_{21} - \boldsymbol{A}_{22}\boldsymbol{W}^{-1}\boldsymbol{L}^T \boldsymbol{F}_1^{-1}\boldsymbol{A}_{11}\right]^T \boldsymbol{\phi}_2 & \\
+ \left[-\boldsymbol{E}_1 - \boldsymbol{A}_{11}^T \boldsymbol{L}^{-T} \boldsymbol{E}_2 \boldsymbol{W}^{-1} \boldsymbol{L}^T \boldsymbol{F}_1^{-1} \boldsymbol{A}_{11}\right] \boldsymbol{\phi}_3 & \\
= \boldsymbol{A}_{11}^T \boldsymbol{L}^{-T}(\boldsymbol{E}_2 \boldsymbol{W}^{-1}(\boldsymbol{z} + \boldsymbol{L}^T \boldsymbol{F}_1^{-1}\boldsymbol{w}) - \boldsymbol{z}) + \boldsymbol{y}. &
\end{aligned}
\tag{37}
$$

This completes the proof because relations (35) and (37) define the $((n_2 + n_3) \times (n_2 + n_3))$ system (14) of Lemma 1.

PROOF THAT B_{11} IS DIAGONAL

Proof.

The matrix $\boldsymbol{L}$ and its inverse, $\boldsymbol{L}^{-1}$ are block diagonal with (possibly signed) unit lower triangular diagonal blocks. As a result the matrix $\boldsymbol{W}^{-1}$ is also block diagonal but with generally full diagonal blocks. Denote $\boldsymbol{R} = \boldsymbol{A}_{22}\boldsymbol{L}^{-1}$. From the formulae in (15) and (16) it follows that $\boldsymbol{B}_{11} = \boldsymbol{F}_2 + \boldsymbol{A}_{22}\boldsymbol{W}^{-1}\boldsymbol{A}_{22}^T = \boldsymbol{F}_2 + \boldsymbol{A}_{22}\left(\boldsymbol{E}_2 + \boldsymbol{L}^T \boldsymbol{F}_1^{-1}\boldsymbol{L}\right)^{-1}\boldsymbol{A}_{22}^T = \boldsymbol{F}_2 + \boldsymbol{A}_{22}\boldsymbol{L}^{-1}\left(\boldsymbol{L}^{-T}\boldsymbol{E}_2\boldsymbol{L}^{-1} + \boldsymbol{F}_1^{-1}\right)^{-1}\boldsymbol{L}^{-T}\boldsymbol{A}_{22}^T = \boldsymbol{F}_2 + \boldsymbol{R}\boldsymbol{U}^{-1}\boldsymbol{R}^T$.

The columns of $\boldsymbol{R}$ are (not necessarily distinct) signed unit vectors. To see this first consider the special case of one of the blocks which will be denoted by $\overline{\boldsymbol{L}} \in \mathbb{R}^{n_4 \times n_4}$, on the diagonal of $\boldsymbol{L}$ and the corresponding submatrix below it, $\overline{\boldsymbol{A}}_{22} \in \mathbb{R}^{n_5 \times n_4}$. The inverse of $\overline{\boldsymbol{L}}$, which must itself be lower triangular, is generally full and the following argument shows that the elements below the diagonal of $\overline{\boldsymbol{L}}^{-1}$ are all in $\{-1, 0, 1\}$. Denote by $\boldsymbol{e}_j$ the jth column of an identity matrix of appropriate dimension, denote the elements of $\overline{\boldsymbol{L}}$ by L_{ij} and consider the solution of the system $\overline{\boldsymbol{L}}\boldsymbol{x} = \boldsymbol{e}_j$ which determines $\boldsymbol{x}$, the j-th column of $\overline{\boldsymbol{L}}^{-1}$. Now, $x_1 = x_2 = \ldots = x_{j-1} = 0$ because $\overline{\boldsymbol{L}}^{-1}$ is lower triangular so $\boldsymbol{e}_j^T \overline{\boldsymbol{L}}\boldsymbol{x} = \boldsymbol{e}_j^T \boldsymbol{e}_j$ reduces to $L_{jj}x_j = 1$ from which it follows that $x_j = L_{jj} = \pm 1$. Suppose now that $x_{j+1}, x_{j+2}, \ldots, x_{j+k-1} \in \{-1, 0, 1\}$, $k > 1$. Then $\boldsymbol{e}_{j+k}^T \overline{\boldsymbol{L}}\boldsymbol{x} = \boldsymbol{e}_{j+k}^T \boldsymbol{e}_j = 0$ which can be written as $L_{j+k,m}x_m + L_{j+k,j+k}x_{j+k} = 0$, some $1 \leq m < j+k$, since

any row of $\overline{L}$ has at most two nonzeros. It follows, since $L_{j+k,j+k} = \pm 1$, that $x_{j+k} = -L_{j+k,j+k}L_{j+k,m}x_m \in \{-1,0,1\}$. Thus, all the elements from the main diagonal down of $\overline{L}^{-1}$ are in $\{-1,0,1\}$ and the diagonal elements of $\overline{L}^{-1}$ are exactly those of $\overline{L}$.

Now, $n_4 - 1$ of the columns of $\overline{A}_{22}$ are zero and just one column, say column m, is an n_5 unit vector, $\widehat{e}_k$, some k. This is because $\overline{A}_{22}$ is the ANIM for the nodes in the internal or external trees which are connected to pipes in the core, i.e. the root nodes of the internal or external trees. Thus, each block of L represents one tree and so has only has one root node and consequently there is exactly one nonzero in A_{22} for each block in L. Then, $\overline{A}_{22} = \widehat{e}_k e_m^T$ and so the product $\overline{R} = \overline{A}_{22}\overline{L} = \widehat{e}_k e_m^T \overline{L}$ is a matrix of the same dimensions as $\overline{A}_{22}$ with the mth row of $\overline{L}$ in its kth row. Thus, $\overline{R}$ is a matrix each column of which is either zero or the same unit vector with possibly different sign and $\overline{R}$ can be written as an algebraic sum of matrices of the form $\widehat{e}_k e_s^T$ for various s.

Suppose now that $\overline{U}^{-1} \in \mathbb{R}^{n_4 \times n_4}$ is the (generally full) diagonal block of $\left(L^{-T}E_2 L^{-1} + F_1^{-1}\right)^{-1}$ which corresponds to $\overline{L}$ and $\overline{A}_{22}$. Then $R\overline{U}^{-1}$ is an algebraic sum of matrices of the form $\widehat{e}_k e_s^T \overline{U}^{-1}$, various s, each of which is a matrix with the sth row of $\overline{U}^{-1}$ in its kth row. As a consequence $\overline{R}\,\overline{U}^{-1}$ is a matrix with zeros everywhere except in the kth row where it has linear combinations of the rows of $\overline{U}^{-1}$. Multiplying $\overline{R}\,\overline{U}^{-1}$ on the right by $\overline{R}^T$, a sum of matrices of the form $e_s \widehat{e}_k^T$, various s, clearly produces a diagonal matrix since all the terms in the sum are products of the form $\widehat{e}_k e_s^T \overline{U}^{-1} e_t \widehat{e}_i^T = \beta \widehat{e}_k \widehat{e}_i$, some scalar β, and all these terms vanish except those for which $k = i$. In other words, only products of the same unit vectors produce terms which are nonzero and those terms are therefore on the diagonal.

Example 3

$$\text{If } \overline{L} = \begin{pmatrix} -1 & 0 & 0 & 0 & 0 \\ 1 & -1 & 0 & 0 & 0 \\ 1 & 0 & -1 & 0 & 0 \\ 0 & 1 & 0 & -1 & 0 \\ 0 & 1 & 0 & 0 & -1 \end{pmatrix} \text{ then } \overline{L}^{-1} = \begin{pmatrix} -1 & 0 & 0 & 0 & 0 \\ -1 & -1 & 0 & 0 & 0 \\ -1 & 0 & -1 & 0 & 0 \\ -1 & -1 & 0 & -1 & 0 \\ -1 & -1 & 0 & 0 & -1 \end{pmatrix}. \tag{38}$$

Suppose that $\widehat{e}_3$ is the third unit vector of dimension four and e_5 is the fifth unit vector of dimension five and that

$$\overline{A}_{22} = \begin{pmatrix} 0 & 0 & 0 & 0 & 0 \\ 0 & 0 & 0 & 0 & 0 \\ 0 & 0 & 0 & 0 & 1 \\ 0 & 0 & 0 & 0 & 0 \end{pmatrix} = \widehat{e}_3 e_5^T.$$

Then the product $\overline{\boldsymbol{A}}_{22}\overline{\boldsymbol{L}}^{-1} = \widehat{\boldsymbol{e}}_3\boldsymbol{e}_5^T\overline{\boldsymbol{L}}$ is a matrix with the fifth row of $\overline{\boldsymbol{L}}^{-1}$ as its third row and zeros elsewhere.

$$\overline{\boldsymbol{R}} = \overline{\boldsymbol{A}}_{22}\overline{\boldsymbol{L}}^{-1} = \begin{pmatrix} 0 & 0 & 0 & 0 & 0 \\ 0 & 0 & 0 & 0 & 0 \\ -1 & -1 & 0 & 0 & -1 \\ 0 & 0 & 0 & 0 & 0 \end{pmatrix} = -\widehat{\boldsymbol{e}}_3\boldsymbol{e}_1^T - \widehat{\boldsymbol{e}}_3\boldsymbol{e}_2^T - \widehat{\boldsymbol{e}}_3\boldsymbol{e}_5^T.$$

Now, if

$$\overline{\boldsymbol{U}}^{-1} = \begin{pmatrix} 4 & 8 & 2 & 1 & 5 \\ 2 & 6 & 3 & 7 & 3 \\ 4 & 4 & 2 & 6 & 5 \\ 4 & 4 & 6 & 7 & 3 \\ 4 & 6 & 1 & 5 & 6 \end{pmatrix} \text{ then } \overline{\boldsymbol{R}U}^{-1} = \begin{pmatrix} 0 & 0 & 0 & 0 & 0 \\ 0 & 0 & 0 & 0 & 0 \\ -10 & -20 & -6 & -13 & -14 \\ 0 & 0 & 0 & 0 & 0 \end{pmatrix}$$
$$= -10\widehat{\boldsymbol{e}}_3\boldsymbol{e}_1^T - 20\widehat{\boldsymbol{e}}_3\boldsymbol{e}_2^T - 6\widehat{\boldsymbol{e}}_3\boldsymbol{e}_3^T - 13\widehat{\boldsymbol{e}}_3\boldsymbol{e}_4^T - 14\widehat{\boldsymbol{e}}_3\boldsymbol{e}_5^T$$

and so

$$\overline{\boldsymbol{R}U}^{-1}\overline{\boldsymbol{R}}^T = \begin{pmatrix} 0 & 0 & 0 & 0 \\ 0 & 0 & 0 & 0 \\ 0 & 0 & 44 & 0 \\ 0 & 0 & 0 & 0 \end{pmatrix} = 44\widehat{\boldsymbol{e}}_3\widehat{\boldsymbol{e}}_3^T.$$

$\square$

Now $\boldsymbol{L}$ has block diagonal form, with lower triangular blocks, and so $\boldsymbol{U}^{-1}$ is block diagonal with generally full diagonal blocks. Thus, the argument above can be applied independently to each block, showing that all the off-diagonal elements of $\boldsymbol{B}_{11}$ vanish. It follows that $\boldsymbol{B}_{11} = \boldsymbol{F}_2 + \boldsymbol{R}\boldsymbol{U}^{-1}\boldsymbol{R}^T$, which is the sum of a non-negative definite term, $\boldsymbol{R}\boldsymbol{U}^{-1}\boldsymbol{R}^T$, and a positive definite diagonal term, $\boldsymbol{F}_2$, is diagonal, positive definite. ∎

PROOF THAT $\boldsymbol{B}_{22}$ IS DIAGONAL

The proof that $\boldsymbol{B}_{22}$ is diagonal relies on the following lemma.

Lemma 7 *Suppose that each column of the matrix $\boldsymbol{A} \in \mathbb{R}^{m \times n}$, is a (possibly signed) unit vector in $\mathbb{R}^m$ (the columns of $\boldsymbol{A}$ need not be distinct). Then, $\boldsymbol{A}\boldsymbol{A}^T$ is diagonal. Moreover, if $\boldsymbol{D} \in \mathbb{R}^{n \times n}$ is a diagonal matrix then $\boldsymbol{A}\boldsymbol{D}\boldsymbol{A}^T$ is also diagonal.*

Proof. Suppose $\{\boldsymbol{e}_i\}, \boldsymbol{e}_i \in \mathbb{R}^m$ and $\{\boldsymbol{u}_i\}, \boldsymbol{u}_i \in \mathbb{R}^n$ are sets of unit vectors and that S is a set of indices $\{s_i\}$, $1 \le s_i \le m$ and T is a set of indices $\{t_i\}$, $1 \le t_i \le n$. The matrix $\boldsymbol{A}$ can be written $\boldsymbol{A} = \sum_{i \in S, j \in T} \boldsymbol{e}_i\boldsymbol{u}_j^T$ where any term $\boldsymbol{u}_j$ can appear in this sum only once since the columns of $\boldsymbol{A}$ are unit vectors. Then, in view of the orthogonality

of the $\boldsymbol{u}_i$, $\boldsymbol{A}\boldsymbol{A}^T = \sum_{i \in S} \alpha_i \boldsymbol{e}_i \boldsymbol{e}_i^T$ where $\boldsymbol{e}_i$ appears α_i times in the sum expression for $\boldsymbol{A}$. Thus, the product is clearly diagonal. ∎

The rest of this section is concerned with the proof that $\boldsymbol{B}_{22}$ is diagonal.

Proof. The matrix $\boldsymbol{B}_{22}$ admits the alternate expression (see Eq. (42))

$$\boldsymbol{B}_{22} = \boldsymbol{E}_1 + \boldsymbol{A}_{11}^T \boldsymbol{F}_1^{-1} \boldsymbol{A}_{11} - \boldsymbol{A}_{11}^T \boldsymbol{F}_1^{-1} \boldsymbol{L} \boldsymbol{W}^{-1} \boldsymbol{L}^T \boldsymbol{F}_1^{-1} \boldsymbol{A}_{11}.$$

The rows of $\boldsymbol{A}_{11}$ are either zero or are (possibly signed) unit vectors (have exactly one nonzero) because $\boldsymbol{L}$ is lower triangular, invertible and $(\begin{array}{cc} \boldsymbol{A}_{11} & \boldsymbol{L} \end{array})$ is part of an ANIM, the rows of which represent links and the columns of which represent vertices. Therefore, in view of Lemma 7, the product $\boldsymbol{A}_{11}^T \boldsymbol{F}_1^{-1} \boldsymbol{A}_{11}$ is diagonal. So, it suffices to show that the term $\boldsymbol{A}_{11}^T \boldsymbol{F}_1^{-1} \boldsymbol{L} \boldsymbol{W}^{-1} \boldsymbol{L}^T \boldsymbol{F}_1^{-1} \boldsymbol{A}_{11}$ is diagonal.

Consider, as in the case of the proof of the diagonality of $\boldsymbol{B}_{11}$, the special case where $\overline{\boldsymbol{L}}$, one of the diagonal blocks of $\boldsymbol{L}$, has the form shown in (38). The first row of $\overline{\boldsymbol{A}}_{11}$, the corresponding submatrix block of $\overline{\boldsymbol{A}}_{11}$, has a single ± 1 and the rest of the matrix is zero and so $\overline{\boldsymbol{A}}_{11} = \boldsymbol{e}_1 \widehat{\boldsymbol{e}}_k^T$ for some k. Consequently, if $\overline{\boldsymbol{F}}_1$ denotes the block of the $\boldsymbol{F}_1$ matrix corresponding to $\overline{\boldsymbol{L}}$, then $\overline{\boldsymbol{A}}_{11} \overline{\boldsymbol{F}}_1^{-1} = \alpha \boldsymbol{e}_1 \widehat{\boldsymbol{e}}_k^T$ for some scalar α. It follows, if $\overline{\boldsymbol{W}}^{-1}$ is the diagonal block of $\boldsymbol{W}^{-1}$ corresponding to $\overline{\boldsymbol{L}}$, that $\alpha^2 \boldsymbol{e}_1 \widehat{\boldsymbol{e}}_k^T \overline{\boldsymbol{L}} \overline{\boldsymbol{W}}^{-1} \overline{\boldsymbol{L}}^T \widehat{\boldsymbol{e}}_k \boldsymbol{e}_1^T$ is a matrix with zeros everywhere with the possible exception of the diagonal element of row 1.

Now, every diagonal block of $\boldsymbol{L}$ has a corresponding submatrix block in $\boldsymbol{A}_{11}$ which has a single nonzero element and the argument above can be applied independently to each block of $\boldsymbol{L}$. Therefore, the matrix $\boldsymbol{B}_{22}$ is the sum of three diagonal terms. In general, $\boldsymbol{B}_{22}$ will not be invertible. ∎

Example 4 Suppose $\overline{\boldsymbol{L}}$ is as in (38), that $\boldsymbol{A}_{11}$ is

$$\boldsymbol{A}_{11} = \widehat{\boldsymbol{e}}_1 \boldsymbol{e}_3^T = \begin{pmatrix} 0 & 0 & 1 & 0 \\ 0 & 0 & 0 & 0 \\ 0 & 0 & 0 & 0 \\ 0 & 0 & 0 & 0 \\ 0 & 0 & 0 & 0 \end{pmatrix} \text{ and that } \overline{\boldsymbol{L}} \overline{\boldsymbol{W}}^{-1} \overline{\boldsymbol{L}}^T = \begin{pmatrix} 2 & 3 & 3 & 3 & 4 \\ 2 & 2 & 4 & 4 & 4 \\ 3 & 1 & 3 & 2 & 3 \\ 1 & 2 & 3 & 5 & 4 \\ 3 & 4 & 2 & 3 & 5 \end{pmatrix}.$$

It follows immediately that

$$\boldsymbol{A}_{11}^T \overline{\boldsymbol{L}} \overline{\boldsymbol{W}}^{-1} \overline{\boldsymbol{L}}^T \boldsymbol{A}_{11} = \widehat{\boldsymbol{e}}_3 \boldsymbol{e}_1^T \overline{\boldsymbol{L}} \overline{\boldsymbol{W}}^{-1} \overline{\boldsymbol{L}}^T \boldsymbol{e}_1 \widehat{\boldsymbol{e}}_3^T = \begin{pmatrix} 0 & 0 & 0 & 0 \\ 0 & 0 & 0 & 0 \\ 0 & 0 & 2 & 0 \\ 0 & 0 & 0 & 0 \end{pmatrix}.$$

836

PROOF THAT $\boldsymbol{S}_H = \boldsymbol{S}_B$

The statement $\boldsymbol{S}_H = \boldsymbol{S}_B$ expands out, on substitution for the various matrices involved, to

$$
\begin{aligned}
\boldsymbol{E}_1 &+ \boldsymbol{A}_{11}^T \boldsymbol{F}_1^{-1} \boldsymbol{A}_{11} + \boldsymbol{A}_{21}^T \boldsymbol{F}_2^{-1} \boldsymbol{A}_{21} \\
&- \left(\boldsymbol{A}_{11}^T \boldsymbol{F}_1^{-1} \boldsymbol{L} + \boldsymbol{A}_{21}^T \boldsymbol{F}_2^{-1} \boldsymbol{A}_{22} \right) \left(\boldsymbol{E}_2 + \boldsymbol{L}^T \boldsymbol{F}_1^{-1} \boldsymbol{L} + \boldsymbol{A}_{22}^T \boldsymbol{F}_2^{-1} \boldsymbol{A}_{22} \right)^{-1} \times \\
& \qquad\qquad\qquad\qquad \left(\boldsymbol{L}^T \boldsymbol{F}_1^{-1} \boldsymbol{A}_{11} + \boldsymbol{A}_{22}^T \boldsymbol{F}_2^{-1} \boldsymbol{A}_{21} \right) \\
&= \boldsymbol{E}_1 + \boldsymbol{A}_{11}^T \boldsymbol{L}^{-T} \boldsymbol{E}_2 \boldsymbol{W}^{-1} \boldsymbol{L}^T \boldsymbol{F}_1^{-1} \boldsymbol{A}_{11} + \\
& \left(\boldsymbol{A}_{21}^T - \boldsymbol{A}_{11}^T \boldsymbol{F}_1^{-1} \boldsymbol{L} \boldsymbol{W}^{-1} \boldsymbol{A}_{22}^T \right) \left(\boldsymbol{F}_2 + \boldsymbol{A}_{22} \boldsymbol{W}^{-1} \boldsymbol{A}_{22}^T \right)^{-1} \times \\
& \qquad\qquad\qquad\qquad \left(\boldsymbol{A}_{21} - \boldsymbol{A}_{22} \boldsymbol{W}^{-1} \boldsymbol{L}^T \boldsymbol{F}_1^{-1} \boldsymbol{A}_{11} \right).
\end{aligned}
$$

The proof is somewhat tedious but straightforward.

Proof. From the definition of $\boldsymbol{H}_{22}$

$$
\begin{aligned}
\boldsymbol{H}_{22} &= \boldsymbol{W} + \boldsymbol{A}_{22}^T \boldsymbol{F}_2^{-1} \boldsymbol{A}_{22} \text{ so} \\
\boldsymbol{A}_{22} \boldsymbol{W}^{-1} \boldsymbol{H}_{22} &= \left(\boldsymbol{F}_2 + \boldsymbol{A}_{22} \boldsymbol{W}^{-1} \boldsymbol{A}_{22}^T \right) \boldsymbol{F}_2^{-1} \boldsymbol{A}_{22} \\
&= \boldsymbol{B}_{11} \boldsymbol{F}_2^{-1} \boldsymbol{A}_{22} \qquad\qquad (39)
\end{aligned}
$$

From the definition of $\boldsymbol{H}_{12}$

$$
\begin{aligned}
\boldsymbol{B}_{12} &= \boldsymbol{A}_{21} - \boldsymbol{A}_{22} \boldsymbol{W}^{-1} (\boldsymbol{H}_{12}^T - \boldsymbol{A}_{22}^T \boldsymbol{F}_2^{-1} \boldsymbol{A}_{21}) \text{ so} \\
\boldsymbol{B}_{11}^{-1} \boldsymbol{B}_{12} &= \boldsymbol{B}_{11}^{-1} (\boldsymbol{A}_{21} + \boldsymbol{A}_{22} \boldsymbol{W}^{-1} \boldsymbol{A}_{22}^T \boldsymbol{F}_2^{-1} \boldsymbol{A}_{21}) - \boldsymbol{F}_2^{-1} \boldsymbol{A}_{22} \boldsymbol{H}_{22}^{-1} \boldsymbol{H}_{12}^T \text{ (using (39))} \\
&= \boldsymbol{F}_2^{-1} \left(\boldsymbol{A}_{21} - \boldsymbol{A}_{22} \boldsymbol{H}_{22}^{-1} \boldsymbol{H}_{12}^T \right) \qquad\qquad (40)
\end{aligned}
$$

Now, multiplying (40) on the left gives

$$
\begin{aligned}
\boldsymbol{A}_{21}^T \boldsymbol{B}_{11}^{-1} \boldsymbol{B}_{12} &= \boldsymbol{A}_{21}^T \boldsymbol{F}_2^{-1} \boldsymbol{A}_{21} - \boldsymbol{A}_{21}^T \boldsymbol{F}_2^{-1} \boldsymbol{A}_{22} \boldsymbol{H}_{22}^{-1} \boldsymbol{H}_{12}^T \\
&= (\boldsymbol{H}_{11} - \boldsymbol{E}_1 - \boldsymbol{A}_{11}^T \boldsymbol{F}_1^{-1} \boldsymbol{A}_{11}) - \boldsymbol{A}_{21}^T \boldsymbol{F}_2^{-1} \boldsymbol{A}_{22} \boldsymbol{H}_{22}^{-1} \boldsymbol{H}_{12}^T \\
&= (\boldsymbol{H}_{11} - \boldsymbol{E}_1 - \boldsymbol{A}_{11}^T \boldsymbol{F}_1^{-1} \boldsymbol{A}_{11}) - (\boldsymbol{H}_{12} - \boldsymbol{A}_{11}^T \boldsymbol{F}_1^{-1} \boldsymbol{L}) \boldsymbol{H}_{22}^{-1} \boldsymbol{H}_{12}^T \\
&= (\boldsymbol{H}_{11} - \boldsymbol{H}_{12} \boldsymbol{H}_{22}^{-1} \boldsymbol{H}_{12}^T) - \boldsymbol{E}_1 - \boldsymbol{A}_{11}^T \boldsymbol{F}_1^{-1} \boldsymbol{A}_{11} + \boldsymbol{A}_{11}^T \boldsymbol{F}_1^{-1} \boldsymbol{L} \boldsymbol{H}_{22}^{-1} \boldsymbol{H}_{12}^T
\end{aligned}
$$

and so

$$\boldsymbol{A}_{21}^T \boldsymbol{B}_{11}^{-1} \boldsymbol{B}_{12} + \boldsymbol{E}_1 + \boldsymbol{A}_{11}^T \boldsymbol{F}_1^{-1} \boldsymbol{A}_{11} - \boldsymbol{A}_{11}^T \boldsymbol{F}_1^{-1} \boldsymbol{L} \boldsymbol{H}_{22}^{-1} \boldsymbol{H}_{12}^T = \boldsymbol{H}_{11} - \boldsymbol{H}_{12} \boldsymbol{H}_{22}^{-1} \boldsymbol{H}_{12}^T \tag{41}$$

The following statements follow from (40):

$$\boldsymbol{A}_{22}^T \boldsymbol{B}_{11}^{-1} \boldsymbol{B}_{12} - \boldsymbol{A}_{22}^T \boldsymbol{F}_2^{-1} \boldsymbol{A}_{21} + \boldsymbol{A}_{22}^T \boldsymbol{F}_2^{-1} \boldsymbol{A}_{22} \boldsymbol{H}_{22}^{-1} \boldsymbol{H}_{12}^T = 0$$

$$\boldsymbol{A}_{22}^T \boldsymbol{B}_{11}^{-1} \boldsymbol{B}_{12} - \boldsymbol{H}_{12}^T + \boldsymbol{A}_{22}^T \boldsymbol{F}_2^{-1} \boldsymbol{A}_{22} \boldsymbol{H}_{22}^{-1} \boldsymbol{H}_{12}^T + \boldsymbol{H}_{12}^T - \boldsymbol{A}_{22}^T \boldsymbol{F}_2^{-1} \boldsymbol{A}_{21} = 0$$

$$\boldsymbol{A}_{22}^T \boldsymbol{B}_{11}^{-1} \boldsymbol{B}_{12} - \boldsymbol{H}_{22} \boldsymbol{H}_{22}^{-1} \boldsymbol{H}_{12}^T + \boldsymbol{A}_{22}^T \boldsymbol{F}_2^{-1} \boldsymbol{A}_{22} \boldsymbol{H}_{22}^{-1} \boldsymbol{H}_{12}^T + \boldsymbol{L}^T \boldsymbol{F}_1^{-1} \boldsymbol{A}_{11} = 0$$

$$\boldsymbol{A}_{22}^T \boldsymbol{B}_{11}^{-1} \boldsymbol{B}_{12} - (\boldsymbol{H}_{22} - \boldsymbol{A}_{22}^T \boldsymbol{F}_2^{-1} \boldsymbol{A}_{22}) \boldsymbol{H}_{22}^{-1} \boldsymbol{H}_{12}^T + \boldsymbol{L}^T \boldsymbol{F}_1^{-1} \boldsymbol{A}_{11} = 0$$

$$\boldsymbol{A}_{22}^T \boldsymbol{B}_{11}^{-1} \boldsymbol{B}_{12} - (\boldsymbol{E}_2 + \boldsymbol{L}^T \boldsymbol{F}_1^{-1} \boldsymbol{L}) \boldsymbol{H}_{22}^{-1} \boldsymbol{H}_{12}^T + \boldsymbol{L}^T \boldsymbol{F}_1^{-1} \boldsymbol{A}_{11} = 0$$

$$\boldsymbol{A}_{22}^T \boldsymbol{B}_{11}^{-1} \boldsymbol{B}_{12} - \boldsymbol{E}_2 \boldsymbol{H}_{22}^{-1} \boldsymbol{H}_{12}^T - \boldsymbol{L}^T \boldsymbol{F}_1^{-1} \boldsymbol{L} \boldsymbol{H}_{22}^{-1} \boldsymbol{H}_{12}^T + \boldsymbol{L}^T \boldsymbol{F}_1^{-1} \boldsymbol{A}_{11} = 0$$

$$\boldsymbol{A}_{22}^T \boldsymbol{B}_{11}^{-1} \boldsymbol{B}_{12} - \boldsymbol{E}_2 \boldsymbol{H}_{22}^{-1} \boldsymbol{H}_{12}^T + \boldsymbol{L}^T \boldsymbol{F}_1^{-1} \boldsymbol{A}_{11} - (\boldsymbol{W} - \boldsymbol{E}_2) \boldsymbol{H}_{22}^{-1} \boldsymbol{H}_{12}^T = 0$$

$$\boldsymbol{A}_{22}^T \boldsymbol{B}_{11}^{-1} \boldsymbol{B}_{12} + \boldsymbol{L}^T \boldsymbol{F}_1^{-1} \boldsymbol{A}_{11} - \boldsymbol{W} \boldsymbol{H}_{22}^{-1} \boldsymbol{H}_{12}^T = 0$$

$$\boldsymbol{A}_{11}^T \boldsymbol{F}_1^{-1} \boldsymbol{L} \boldsymbol{W}^{-1} \boldsymbol{A}_{22}^T \boldsymbol{B}_{11}^{-1} \boldsymbol{B}_{12} + \boldsymbol{A}_{11}^T \boldsymbol{F}_1^{-1} \boldsymbol{L} \boldsymbol{W}^{-1} \boldsymbol{L}^T \boldsymbol{F}_1^{-1} \boldsymbol{A}_{11} - \boldsymbol{A}_{11}^T \boldsymbol{F}_1^{-1} \boldsymbol{L} \boldsymbol{H}_{22}^{-1} \boldsymbol{H}_{12}^T = 0$$

$$(\boldsymbol{A}_{21}^T - \boldsymbol{B}_{12}^T) \boldsymbol{B}_{11}^{-1} \boldsymbol{B}_{12} + \boldsymbol{A}_{11}^T \boldsymbol{F}_1^{-1} \boldsymbol{L} \boldsymbol{W}^{-1} \boldsymbol{L}^T \boldsymbol{F}_1^{-1} \boldsymbol{A}_{11} - \boldsymbol{A}_{11}^T \boldsymbol{F}_1^{-1} \boldsymbol{L} \boldsymbol{H}_{22}^{-1} \boldsymbol{H}_{12}^T = 0$$

$$\boldsymbol{A}_{21}^T \boldsymbol{B}_{11}^{-1} \boldsymbol{B}_{12} - \boldsymbol{B}_{12}^T \boldsymbol{B}_{11}^{-1} \boldsymbol{B}_{12} + \boldsymbol{A}_{11}^T \boldsymbol{F}_1^{-1} \boldsymbol{L} \boldsymbol{W}^{-1} \boldsymbol{L}^T \boldsymbol{F}_1^{-1} \boldsymbol{A}_{11} - \boldsymbol{A}_{11}^T \boldsymbol{F}_1^{-1} \boldsymbol{L} \boldsymbol{H}_{22}^{-1} \boldsymbol{H}_{12}^T = 0$$

Thus, $\boldsymbol{B}_{22} + \boldsymbol{A}_{21}^T \boldsymbol{B}_{11}^{-1} \boldsymbol{B}_{12} + \boldsymbol{A}_{11}^T \boldsymbol{F}_1^{-1} \boldsymbol{L} \boldsymbol{W}^{-1} \boldsymbol{L}^T \boldsymbol{F}_1^{-1} \boldsymbol{A}_{11} - \boldsymbol{A}_{11}^T \boldsymbol{F}_1^{-1} \boldsymbol{L} \boldsymbol{H}_{22}^{-1} \boldsymbol{H}_{12}^T = \boldsymbol{B}_{22} + \boldsymbol{B}_{12}^T \boldsymbol{B}_{11}^{-1} \boldsymbol{B}_{12}$ and the result is proved if it can be shown, in view of (41), that

$$\boldsymbol{B}_{22} + \boldsymbol{A}_{21}^T \boldsymbol{B}_{11}^{-1} \boldsymbol{B}_{12} + \boldsymbol{A}_{11}^T \boldsymbol{F}_1^{-1} \boldsymbol{L} \boldsymbol{W}^{-1} \boldsymbol{L}^T \boldsymbol{F}_1^{-1} \boldsymbol{A}_{11} - \boldsymbol{A}_{11}^T \boldsymbol{F}_1^{-1} \boldsymbol{L} \boldsymbol{H}_{22}^{-1} \boldsymbol{H}_{12}^T =$$
$$\boldsymbol{A}_{21}^T \boldsymbol{B}_{11}^{-1} \boldsymbol{B}_{12} + \boldsymbol{E}_1 + \boldsymbol{A}_{11}^T \boldsymbol{F}_1^{-1} \boldsymbol{A}_{11} - \boldsymbol{A}_{11}^T \boldsymbol{F}_1^{-1} \boldsymbol{L} \boldsymbol{H}_{22}^{-1} \boldsymbol{H}_{12}^T$$

or that $\boldsymbol{B}_{22} = \boldsymbol{E}_1 + \boldsymbol{A}_{11}^T \boldsymbol{F}_1^{-1} \boldsymbol{A}_{11} - \boldsymbol{A}_{11}^T \boldsymbol{F}_1^{-1} \boldsymbol{L} \boldsymbol{W}^{-1} \boldsymbol{L}^T \boldsymbol{F}_1^{-1} \boldsymbol{A}_{11}$. Now, $\boldsymbol{I} - \boldsymbol{F}_1^{-1} \boldsymbol{L} \boldsymbol{W}^{-1} \boldsymbol{L}^T = \boldsymbol{L}^{-T} \boldsymbol{L}^T - \boldsymbol{F}_1^{-1} \boldsymbol{L} \boldsymbol{W}^{-1} \boldsymbol{L}^T = \boldsymbol{L}^{-T} \left(\boldsymbol{W} - \boldsymbol{L}^T \boldsymbol{F}_1^{-1} \boldsymbol{L} \right) \boldsymbol{W}^{-1} \boldsymbol{L}^T = \boldsymbol{L}^{-T} \boldsymbol{E}_2 \boldsymbol{W}^{-1} \boldsymbol{L}^T$ and multiplying on the right by $\boldsymbol{F}_1^{-1} \boldsymbol{A}_{11}$ gives

$$\boldsymbol{F}_1^{-1} \boldsymbol{A}_{11} - \boldsymbol{F}_1^{-1} \boldsymbol{L} \boldsymbol{W}^{-1} \boldsymbol{L}^T \boldsymbol{F}_1^{-1} \boldsymbol{A}_{11} = \boldsymbol{L}^{-T} \boldsymbol{E}_2 \boldsymbol{W}^{-1} \boldsymbol{L}^T \boldsymbol{F}_1^{-1} \boldsymbol{A}_{11}$$

$$\boldsymbol{A}_{11}^T \boldsymbol{F}_1^{-1} \boldsymbol{A}_{11} - \boldsymbol{A}_{11}^T \boldsymbol{F}_1^{-1} \boldsymbol{L} \boldsymbol{W}^{-1} \boldsymbol{L}^T \boldsymbol{F}_1^{-1} \boldsymbol{A}_{11} = \boldsymbol{A}_{11}^T \boldsymbol{L}^{-T} \boldsymbol{E}_2 \boldsymbol{W}^{-1} \boldsymbol{L}^T \boldsymbol{F}_1^{-1} \boldsymbol{A}_{11}$$

$$\boldsymbol{E}_1 + \boldsymbol{A}_{11}^T \boldsymbol{F}_1^{-1} \boldsymbol{A}_{11} - \boldsymbol{A}_{11}^T \boldsymbol{F}_1^{-1} \boldsymbol{L} \boldsymbol{W}^{-1} \boldsymbol{L}^T \boldsymbol{F}_1^{-1} \boldsymbol{A}_{11} = \boldsymbol{E}_1 + \boldsymbol{A}_{11}^T \boldsymbol{L}^{-T} \boldsymbol{E}_2 \boldsymbol{W}^{-1} \boldsymbol{L}^T \boldsymbol{F}_1^{-1} \boldsymbol{A}_{11} \tag{42}$$

$$= \boldsymbol{B}_{22} \tag{43}$$

and the result is proved. ∎

SUMMARY OF THE PROCESS TO DETERMINE B, THE JACOBIAN OF THE TOPOLOGICAL MINOR

In this section we summarize the process of permuting the ANIM and finding the matrices which define the topological minor.

Given the block matrices $\boldsymbol{F}$, $\boldsymbol{E}$ and $\boldsymbol{A}$ in (3):

(a) Use the FCPA, which is described in Simpson et al. (2014), to produce the row and column permutations $\widetilde{\boldsymbol{P}}$ and $\widetilde{\boldsymbol{R}}$ of (9) which, when applied to $\boldsymbol{A}$, partition the forest element of the network from the core.

(b) Use the GMPA, which is described in Deuerlein et al. (2016), to find the permutations $\widehat{\boldsymbol{P}}$ and $\widehat{\boldsymbol{R}}$ of (10) which, when applied to the ANIM of the core $\widetilde{\boldsymbol{A}}_{21}$, identify the topological minor and partition it from the internal forest.

(c) Integrate the permutations $\widetilde{\boldsymbol{P}}$, $\widehat{\boldsymbol{P}}$ and $\widetilde{\boldsymbol{R}}$, $\widehat{\boldsymbol{R}}$.

(d) Apply the Schilders factoring, described in Elhay et al. (2014) to find the permutations $\overline{\boldsymbol{P}}$ and $\overline{\boldsymbol{R}}$ of (11).

(e) Integrate the permutation $\overline{\boldsymbol{P}}$ and $\overline{\boldsymbol{R}}$ with those of step (c) to find the overall permutations $\boldsymbol{P}$ and $\boldsymbol{R}$ which give the final form (8).

(f) Use the scheme described in the section headed "Efficient calculation of the diagonal matrices $\boldsymbol{B}_{11}$ and $\boldsymbol{B}_{22}$" to compute the matrices which make up the topological minor and which are defined in (15) to (18). This completes the computation of the matrix $\boldsymbol{B}$ of (21).

(g) The Schur complement, $\boldsymbol{S}_B$, of the topological minor can be computed, if required, using (23).

(h) The quantities $\phi_{1,2,3,4}$ of (13) can be computed, if required, using the results of Lemma 2 and Lemma 3.

NUMERICAL CONSIDERATIONS AND SOFTWARE

All the calculations reported in this paper were done using a suite of codes specially written by the first author for Matlab, (Mathworks 2016) which exploit the sparse matrix arithmetic facilities available in that package. Four Matlab Mex files which are C implementations of four of the Matlab programming language codes in the suite were used. Matlab arithmetic conforms to the IEEE Double Precision Standard and so machine epsilon for all these calculations was 2.2×10^{-16}. The Matlab software was run on a PC with a Windows 7, 64-bit operating system with an i7-4700MQ processor.

SUPPLEMENTAL DATA

The data files for some of the networks in this paper are publicly available:

(a) The EPANET `.inp` files for the network shown in Fig. 1 and the networks N_1, N_3, N_4 and N_7 which are listed in Table 7 is avialable online in the ASCE Library (www.ascelibrary.org). The other four networks N_2, N_5, N_6 and N_8 are not freely available either because they are proprietary or because of security concerns.

(b) The EPANET `.inp` file for the Balerma network is available from
http://emps.exeter.ac.uk/engineering/research/cws/resources/
benchmarks/design-resiliance-pareto-fronts/data-files/.

TABLES AND FIGURES

$$A = $$

	v_1	v_2	v_3	v_4	v_5	v_6	v_7	v_8	v_9	v_{10}	v_{11}
p_1	-1	0	0	0	0	0	0	0	0	0	0
p_2	1	0	-1	0	0	0	0	0	0	0	0
p_3	0	0	1	-1	0	0	0	0	0	0	0
p_4	1	0	0	0	-1	0	0	0	0	0	0
p_5	1	0	0	0	0	-1	0	0	0	0	0
p_6	0	0	0	0	0	1	-1	0	0	0	0
p_7	0	0	0	0	0	0	1	-1	0	0	0
p_8	0	-1	0	0	1	0	0	0	0	0	0
p_9	0	-1	0	1	0	0	0	0	0	0	0
p_{10}	0	-1	0	0	0	0	0	1	0	0	0
p_{11}	0	0	0	-1	0	0	0	0	1	0	0
p_{12}	0	0	0	0	0	0	0	-1	0	1	0
p_{13}	0	0	0	-1	0	0	0	0	0	0	1

Table 1: The ANIM for the network in Fig. 1 before permutation into the form shown in Fig. 4. The links (pipes) are labeled p_i and the vertices (nodes) are labeled v_i

$$\widetilde{P} A \widetilde{R} = \begin{matrix} \widetilde{n}_1 \\ \widetilde{n}_2 \end{matrix} \begin{pmatrix} \widetilde{A}_{11} & \widetilde{L} \\ \widetilde{A}_{21} & O \end{pmatrix} = $$

	v_1	v_2	v_3	v_4	v_5	v_6	v_7	v_8	v_9	v_{10}	v_{11}
p_{11}	0	0	0	-1	0	0	0	0	1	0	0
p_{12}	0	0	0	0	0	0	0	-1	0	1	0
p_{13}	0	0	0	-1	0	0	0	0	0	0	1
p_1	-1	0	0	0	0	0	0	0	0	0	0
p_2	1	0	-1	0	0	0	0	0	0	0	0
p_3	0	0	1	-1	0	0	0	0	0	0	0
p_4	1	0	0	0	-1	0	0	0	0	0	0
p_5	1	0	0	0	0	-1	0	0	0	0	0
p_6	0	0	0	0	0	1	-1	0	0	0	0
p_7	0	0	0	0	0	0	1	-1	0	0	0
p_8	0	-1	0	0	1	0	0	0	0	0	0
p_9	0	-1	0	1	0	0	0	0	0	0	0
p_{10}	0	-1	0	0	0	0	0	1	0	0	0

Table 2: The ANIM for the network in Fig. 1 after FCPA permutation into the form shown in (9). The links (pipes) are labeled p_i and the vertices (nodes) are labeled v_i. Here $\widetilde{n}_1 = 3$, $\widetilde{n}_2 = 10$ and $\widetilde{n}_3 = 8$.

$$\widehat{\boldsymbol{P}}\widetilde{\boldsymbol{A}}_{21}\widehat{\boldsymbol{R}} = \begin{matrix}\widehat{n}_1\\\widehat{n}_2\end{matrix}\begin{pmatrix}\widehat{\boldsymbol{A}}_{11} & \widehat{\boldsymbol{L}}\\ \widehat{\boldsymbol{A}}_{21} & \widehat{\boldsymbol{A}}_{22}\end{pmatrix} =$$

	v_1	v_2	v_3	v_4	v_5	v_6	v_7	v_8
p_2	1	0	-1	0	0	0	0	0
p_3	0	0	1	-1	0	0	0	0
p_4	1	0	0	0	-1	0	0	0
p_5	1	0	0	0	0	-1	0	0
p_6	0	0	0	0	0	1	-1	0
p_7	0	0	0	0	0	0	1	-1
p_1	-1	0	0	0	0	0	0	0
p_8	0	-1	0	0	1	0	0	0
p_9	0	-1	0	1	0	0	0	0
p_{10}	0	-1	0	0	0	0	0	1

Table 3: The GMPA permuted ANIM $\widetilde{\boldsymbol{A}}_{21}$ for the core of the network in Fig. 1. It has the form shown in (10). The links (pipes) are labeled p_i and the vertices (nodes) are labeled v_i. Here $\widehat{n}_1 = 6$, $\widehat{n}_2 = 4$ and $\widehat{n}_3 = 2$.

$$\begin{pmatrix}\widetilde{\boldsymbol{A}}_{11\_b} & \widetilde{\boldsymbol{L}}\\ \widehat{\boldsymbol{L}} & \boldsymbol{O}\\ \widehat{\boldsymbol{A}}_{22} & \end{pmatrix} =$$

	v_3	v_4	v_5	v_6	v_7	v_8	v_9	v_{10}	v_{11}
p_{11}	0	-1	0	0	0	0	1	0	0
p_{12}	0	0	0	0	0	-1	0	1	0
p_{13}	0	-1	0	0	0	0	0	0	1
p_2	-1	0	0	0	0	0	0	0	0
p_3	1	-1	0	0	0	0	0	0	0
p_4	0	0	-1	0	0	0	0	0	0
p_5	0	0	0	-1	0	0	0	0	0
p_6	0	0	0	1	-1	0	0	0	0
p_7	0	0	0	0	1	-1	0	0	0
p_1	0	0	0	0	0	0	0	0	0
p_8	0	0	1	0	0	0	0	0	0
p_9	0	1	0	0	0	0	0	0	0
p_{10}	0	0	0	0	0	1	0	0	0

Table 4: The submatrix shown on the left of (11) for the network of Fig. 1 before the Schilders permutation into the form shown in on the right of (11). The links (pipes) are labeled p_i and the vertices (nodes) are labeled v_i.

$$\boldsymbol{PAR} = \begin{matrix}n_1\\n_2\end{matrix}\begin{pmatrix}\boldsymbol{A}_{11} & \boldsymbol{L}\\ \boldsymbol{A}_{21} & \boldsymbol{A}_{22}\end{pmatrix} =$$

	v_1	v_2	v_3	v_4	v_{11}	v_9	v_5	v_6	v_7	v_8	v_{10}
p_2	1	0	-1	0	0	0	0	0	0	0	0
p_3	0	0	1	-1	0	0	0	0	0	0	0
p_{13}	0	0	0	-1	1	0	0	0	0	0	0
p_{11}	0	0	0	-1	0	1	0	0	0	0	0
p_4	1	0	0	0	0	0	-1	0	0	0	0
p_5	1	0	0	0	0	0	0	-1	0	0	0
p_6	0	0	0	0	0	0	0	1	-1	0	0
p_7	0	0	0	0	0	0	0	0	1	-1	0
p_{12}	0	0	0	0	0	0	0	0	0	-1	1
p_1	-1	0	0	0	0	0	0	0	0	0	0
p_8	0	-1	0	0	0	0	1	0	0	0	0
p_9	0	-1	0	1	0	0	0	0	0	0	0
p_{10}	0	-1	0	0	0	0	0	0	0	1	0

Table 5: The final ANIM for the network in Fig. 1 after permutation with the FCPA and GMPA into the form shown in Fig. 4. The links (pipes) are labeled p_i and the vertices (nodes) are labeled v_i. Here $n_1 = 9$, $n_2 = 4$ and $n_3 = 2$

i	q_i (L/s)	h_i (m)	$\omega(h_i)$ (L/s)	d_i (L/s)	$\frac{\omega(h_i)}{d_i}\%$
1	238.2	12.9	35.6	50.0	71.2
2	68.3	8.4	19.1	50.0	38.3
3	44.4	9.7	23.9	50.0	47.9
4	67.8	8.3	18.8	50.0	37.7
5	66.6	9.8	24.1	50.0	48.2
6	42.0	9.9	24.5	50.0	49.1
7	22.1	8.6	19.9	50.0	39.8
8	43.7	8.3	18.6	50.0	37.2
9	-10.3	8.1	17.9	50.0	35.9
10	-14.2	8.0	17.7	50.0	35.4
11	-17.9	8.1	17.9	50.0	35.9
12	-17.7	$-$	$-$	$-$	$-$
13	-17.9	$-$	$-$	$-$	$-$

Table 6: The steady state flows, q_i, heads h_i, the nodal deliveries, $\omega(h_i)$, the demands, d_i and nodal deliveries as precentages of demands for the network shown in Fig. 1.

ID	n_p	n_j	n_1	n_2	n_3	nnz($\boldsymbol{B}_{11}$)	nnz($\boldsymbol{H}_{22}$)	$\frac{nnz(\boldsymbol{B}_{11})}{nnz(\boldsymbol{H}_{22})}\%$
N_1	934	848	688	246	160	246	1816	14
N_2	1118	1039	883	235	156	235	2255	10
N_3	1976	1770	1429	547	341	547	3597	15
N_4	2465	1890	1086	1379	804	1379	2134	65
N_5	2508	2443	2321	187	122	187	6591	3
N_6	8584	8392	8042	542	350	542	23016	2
N_7	14830	12523	8425	6405	4098	6405	19819	32
N_8	19647	17971	14769	4878	3202	4878	36609	13

Table 7: The number of nonzeros in the matrices $\boldsymbol{B}_{11}$ and $\boldsymbol{H}_{22}$ for the eight case study networks when both the FCPA and GMPA permutations were used.

	d_1	d_2	d_3	d_4	d_5	d_6	d_7	d_8	d_9	d_{10}	d_{11}
h_1	-21.4	-7.1	-9.3	-6.3	-11.4	-8.6	-4.4	-3.4	-5.0	-3.0	-5.6
h_2	-13.1	-14.1	-10.8	-9.9	-12.3	-5.9	-3.9	-3.9	-7.8	-3.5	-8.8
h_3	-13.8	-8.6	-19.5	-10.5	-9.5	-5.8	-3.3	-2.9	-8.3	-2.7	-9.3
h_4	-12.0	-10.1	-13.4	-13.3	-9.7	-5.2	-3.2	-3.0	-10.5	-2.7	-11.8
h_5	-16.8	-9.7	-9.5	-7.6	-17.6	-7.0	-4.0	-3.4	-5.9	-3.1	-6.7
h_6	-12.4	-4.6	-5.7	-4.0	-6.9	-29.3	-13.0	-8.2	-3.1	-7.4	-3.6
h_7	-7.8	-3.8	-4.0	-3.1	-4.8	-16.0	-25.8	-15.6	-2.4	-14.1	-2.7
h_8	-6.4	-4.0	-3.8	-3.1	-4.5	-10.8	-16.7	-23.6	-2.4	-21.3	-2.7
h_9	-9.9	-8.3	-11.0	-11.0	-8.0	-4.3	-2.7	-2.5	-26.1	-2.3	-9.7
h_{10}	-6.1	-3.8	-3.6	-2.9	-4.2	-10.2	-15.8	-22.3	-2.3	-25.4	-2.6
h_{11}	-11.1	-9.4	-12.4	-12.4	-9.0	-4.9	-3.0	-2.8	-9.7	-2.5	-17.9

Table 8: The PDM first order steady-state sensitivities of heads, h_i, in the network shown in Fig. 1 to the nodal demands, d_i. Unlike the case for DDM, this PDM sensitivity matrix is not symmetric.
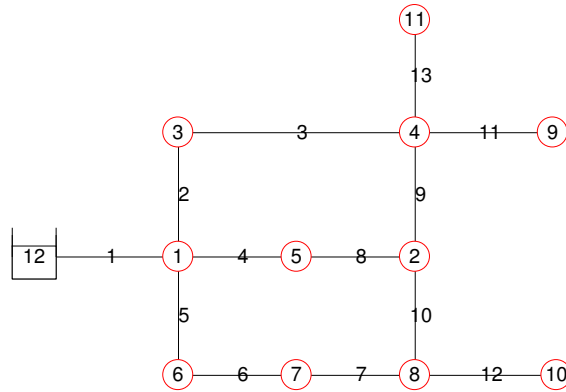

Figure 1: The example network used to illustrate the partitioning scheme. It is a network from Deuerlein et al. (2016) but with an external forest added.
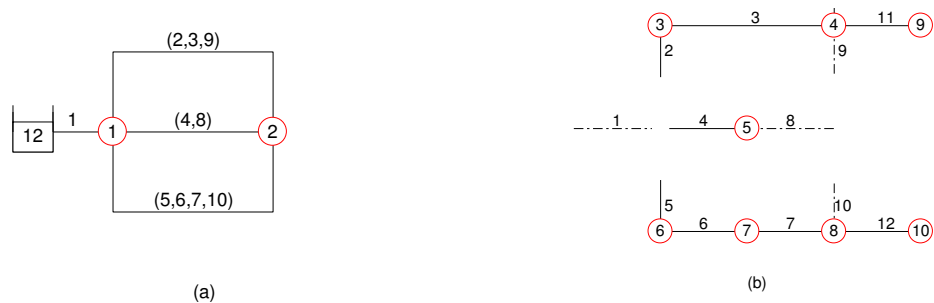
Figure 2: (a) The topological minor of the example network of Fig. 1 showing the internal tree branches and chords (in parentheses) which underlie the superlinks, and (b) the corresponding internal and external forest elements together with the internal cotree chords. The internal tree chords (links 1, 8, 9, 10) are shown with dashed lines.
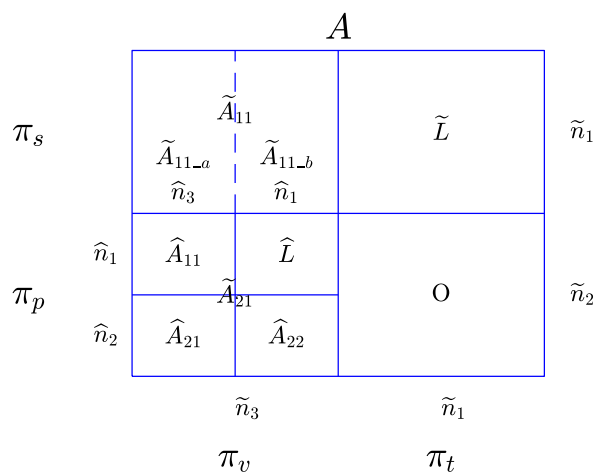
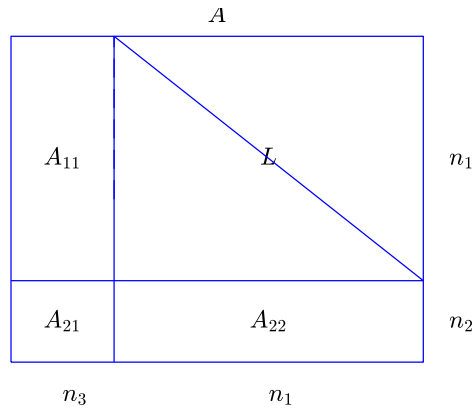Figure 3: An arc-node incidence matrix $\boldsymbol{A}$ showing both the FCPA partitioning ($\sim$) and the GMPA partitioning ($\widehat{}$).

Figure 4: An arc-node incidence matrix $\boldsymbol{A}$ showing the final partitioning after the FCPA and GMPA permutations have been applied.
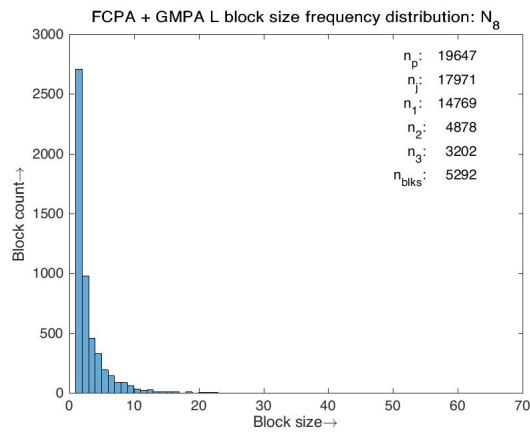
Figure 5: The frequency distribution of block sizes for the largest case study network N_8 used in this paper. The matrix $\boldsymbol{W}^{-1}$ for this network has $n_{blks} = 5,292$ blocks on the diagonal.
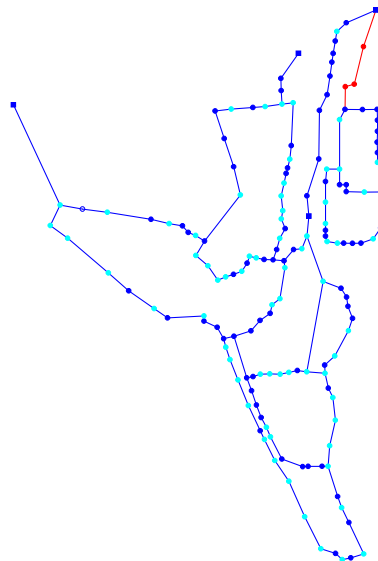
Figure 6: The full Balerma network

Figure 7: The core of the Balerma network after the FCPA has been applied. The cyan coloured nodes are the root nodes of trees in the external forest, the red nodes are the internal bridge nodes and the remaining nodes (and sources) are blue.
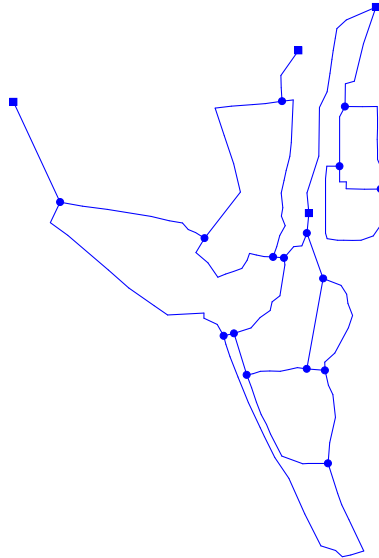
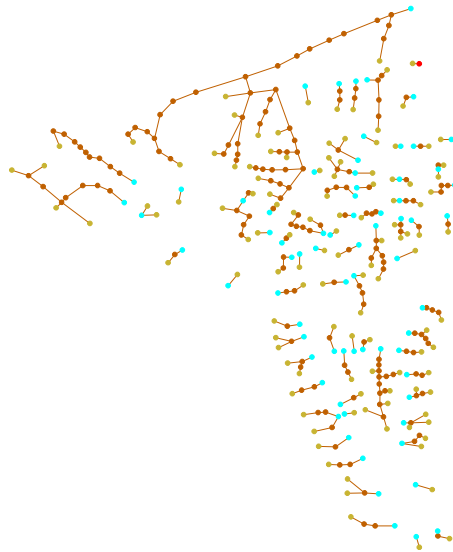Figure 8: The topological minor of the Balerma network

Figure 9: The Balerma network's external forest. The cyan coloured nodes are the external forest's root nodes, the the light brown nodes are leaves of the external forest trees and the remaining nodes of the external forest are, apart from the single red node which connects a tree to a bridge, dark brown.